Czech Technical University
Faculty of Nuclear Sciences and Physical Engineering
Department of Physics

Study of the coupling properties of a Passive-Active Multijunction Lower Hybrid antenna with tokamak plasma

Diploma thesis

Author: Michal Kazda
Supervisor: Ing. František Žáček, CSc.
Submitted: 06.05.2011

Prohlášení

Prohlašuji, že jsem svou diplomovou práci vypracoval samostatně a použil jsem pouze podklady (literaturu, projektz, SW atd.) uvedené v přiloženém seznamu. Nemám závažný důvod proti užití tohoto školního díla ve smyslu §60 Zákona č.121/2000 Sb., o právu autorském, o právech souvisejících s právem autorským a o změně některých zákonů (autorský zákon).

V Praze dne.....................

Michal Kazda

Acknowledgments

For really the first place, I would like to deeply thank to Ing. František Žáček, CSc., who followed and guided my university study for couple of last years. From pretty beginnings till these days, he was helping me with all study issues I was dealing with. Starting with my bachelor thesis, he led myself to the rest of my stay at the Czech Technical University. I thank him also for his great patience. My gratitude belongs also to Ing. Vojtěch Svoboda, CSc. and RNDr. Jan Mlynář, Ph.D., leaders of Physics and Technology of Thermonuclear Fusion branch of study for organization, many helps and guidance during my whole study. Next deep acknowledgments are for Dr. Julien Hillairet, who was leading all my work I spent in CEA, Cadarache in France. Since this is also the last opportunity to thank during my university studies, I want to last but not least thank my parents and family for many years of broadest support and confidence to prosperous graduation.

Název práce: **Studium vlastností navázání plazmatu v tokamaku s pasivní-aktivní mnohaspojnou dolnohybridní anténou**

Author: Michal Kazda

Obor: Fyzikální inženýrství

Druh práce: Diplomová práce

Vedoucí práce: Ing. František Žáček, CSc., oddělení Tokamak, Ústav Fyziky Plazmatu, Akademie věd České republiky, v.v.i.

Abstrakt: Esenciální problém, který bude muset být vyřešen v budoucím prototypu elektrárny pracující na principu Tokamaku, je dosažení kontinuálního provozu. Tokamak je totiž principiálně pulzní zařízení. LHCD (Lower Hybrid Current Drive), označení pro dolnohybridní vlečení proudu, nabízí potenciál možnosti řešení tohoto problému. To spočívá ve vyzařování elektromagnetických vln do plazmatu v komoře tokamaku pomocí speciální vyzařovací struktury – LH antény. Studiem navázání plazmatu v tokamaku s dolnohybridní anténou se zabývá výpočetní kód ALOHA. Předmětem této diplomové práce je implementace plug-in modulu HAMAC, který popisuje radiofrekvenční charakterizaci antény a je nezbytnou součástí kódu ALOHA. Součástí kódu HAMAC je také série optimizačních programů, pomocí kterých jsou představeny návrhy dvou konceptů dolnohybridní antény na frekvenci 3.7GHz pro český tokamak COMPASS.

Klíčová slova: HAMAC, rozptylová matice, dolnohybridní anténa, TE a TM mód, vlnovod.

title: **Study of the coupling properties of a Passive-Active Multijunction Lower Hybrid antenna with tokamak plasma**

Author: Michal Kazda

Abstract: A key issue to be solved on the future power plant prototype based on a tokamak principle is a steady state operation. In principle, tokamak is a pulse device. LHCD (lower hybrid current drive) shows a potential of possible solution of this problem. It consists of electromagnetic wave radiation into the plasma inside a tokamak by means of a specific radiation aperture – LH antenna. The ALOHA code is dealing with the study of the coupling of the plasma and the LH antenna. The aim of this thesis is the implementation of HAMAC code, plug-in code, which gives a RF characterization of an antenna and is a component of ALOHA code. A part of HAMAC is a set of optimization programs. With the help of HAMAC, two designs of scheduled LH 3,7GHz antenna are presented.

Key words: HAMAC, scattering matrix, Lower hybrid antenna, TE and TM modes, waveguide.

Contents

Chapter 1

Introduction

It took almost 60 years since the research of peaceful usage of thermonuclear fusion reaction triggered. Nevertheless, when construction of the International Thermonuclear Experimental Reactor (ITER) started in 2007 in Cadarache, France, scientists are about to reach one of the milestones in this research - for the first time, thermonuclear fusion reactor should with estimated thermal power of 500MW produce more energy than needed for the reaction sustenance. To do so, dimensions of the reactor vessel need to be doubled with respect to present largest experiment and also the duration of the pulse need to be sufficiently long ($15 - 30$min.). ITER will be a tokamak reactor, which indicates the needfulness of electrical current presence in plasma in toroidal direction. One of the external method for generation (and preservation) of this current is a usage of powerful electromagnetic waves, which having specific parameters are injected to the reactor plasma via a specific launching structure called a LHCD antenna (LHCD reads Lower Hybrid Current Drive). Such waves are effective in impulse transfer and thus energy to electrons in plasma. This lead to desired electrical current in the toroidal direction. Anyhow there are some issues with the LHCD current drive usage, namely the effectivity of the coupling of the radiated power to the plasma and the mitigation of the reflected power coming back to the antenna. Advanced LOwer Hybrid Antenna - ALOHA code was developed in CEA IRFM (Institut de Recherche sur la Fusion Magnetique) in Cadarache to study these issues. For this purpose, the antenna radio frequency characteristics needs to be know. Preliminary, the commercial 3D full-wave SW ANSYS HFSS was used for calculation of scattering matrix (S - matrix) and optimization of LHCD antenna. This thesis presents the plug-in module HAMAC (Hybrid Antenna Modeling for the ALOHA Code) which I developed in order to be a supplement for HFSS software. Goal of this module is to calculate a scattering matrix of so-called multijunction antenna, i.e. a LHCD antenna. HAMAC module contains number of optimization tools for the design of multijunction antenna optimization too. Work is based on upgrade of the HAMAC when preliminary, only Transverse electric (TE) modes of propagating electromagnetic waves were considered, to the complex approach with Transverse magnetic (TM) modes too.

This thesis is based on the long time LHCD system study study [11, 14, 13, 12]. In the introduction chapter of this thesis, I am presenting basic features of the topic. Step-by-step I present concept of thermonuclear fusion, tokamak description and give an overview of several options of electrical current generation in tokamaks. Further, LHCD as a tool for steady state current generation in tokamak plasma is introduced with several examples. Last part of this intro chapter is dealing with description of ALOHA code. ALOHA code needs as one of inputs the S - matrix to be calculated by module HAMAC. Code is still upgraded and used now for design development of LHCD antenna for ITER.

Second chapter provides complex description of HAMAC code with the presentation of the calculus method and explanation of the basic philosophy of a mode-matching approach. The last chapter presents the results of the work. Beside the examples of optimization results of different parts of multijunction antenna, the mechanism of importance of TM modes in calculus is presented. Validation of the HAMAC code by comparison with HFSS SW results for real LH antenna under operation on EAST tokamak placed in IPP Hefei, China, is performed. Based on that, the HAMAC code is used for design proposal of future Prague COMPASS tokamak LH antenna. The attention is focused to the comparison of results obtained by HAMAC module and by HFSS software. Good agreement is observed only when both TE and TM modes are considered in calculus even if in the design, all TM modes are evanescent and can not propagate through an antenna.

1.1 Basics of thermonuclear fusion

An exquisite general introduction to the thermonuclear fusion can be found in [**?**]. Nuclear fusion is a nuclear reaction when two light elements collapses together to form one heavier nucleus. The sum of mass of output elements is smaller than total mass of nucleus entering the reaction. The net energy release appears. To force two nucleus to collapses, the repulsive Coulomb force needs to be overcame. In the core of stars, giant gravity forces serves this purpose, whereas in terrestrial conditions, this is not a case. Only way is to use a kinetic energy of chaotic thermal motion of particles to be collapsed. The demanded internal energy is still several tens of keV, this is several hundreds of millions of Kelvin. Compare with core temperature in the sun being around 15mil. of Kelvin. All matter with such a temperature is in a state of fully ionized plasma. It is possible to define a plasma as a quasi-neutral mixture of freely moving positive and negative charged elements with a collective behavior. Charged particles generate during its thermal motion and mutual collisions local failure of charge concentration and thus electric neutrality. These local electric fields influence other charged particles. This explains the word “collective” in the definition of plasma. the temperature of plasma is in a broad interval from 10000K in TV screens to hundreds of millions of K in fusion. In plasma physics, the temperature is usually expressed in energy units via the formula $E = kT$ where $k = 1.38 \cdot 10^{-23}$J/K is a Boltzmann constant. Re-computation of the temperature reads:

$$1\text{eV} = (e/k)\text{K} \simeq 11600\text{K}.$$

Plasma is able to attenuate the electrical potential put into the plasma. This effect is called a Debay shielding. The potential put into the plasma will attract the opposite charged particles only to the radius where the potential energy balance the particle thermal energy. The thickness of this particle shielding cloud [4] is

$$\lambda_D = \left(\frac{\epsilon_0 k T_e}{n e^2}\right)^{\frac{1}{2}}, \tag{1.1}$$

where n is a density, T_e is an electron temperature, k is Boltzmann constant and finally ϵ_0 is the vacuum permittivity. λ_D is called a Debye length. In its definition, only a electron temperature is present, because electrons are more moveable and thus exclusively acts in Debye shielding process. The “quasi-neutrality” word in plasma definition could be defined with the help of Debay length in the way that the ionized gas can be labeled as a plasma only if $L \ggg \lambda_D$ where L is a typical size of studied area. To finish full explanation of our definition of the term plasma, we can state that the number of particles in a Debye cloud is

$$N_D = n\frac{4}{3}\pi\lambda_D^3 = 1.38 \cdot 10^6 \frac{T^{3/2}}{n^{1/2}} \tag{1.2}$$

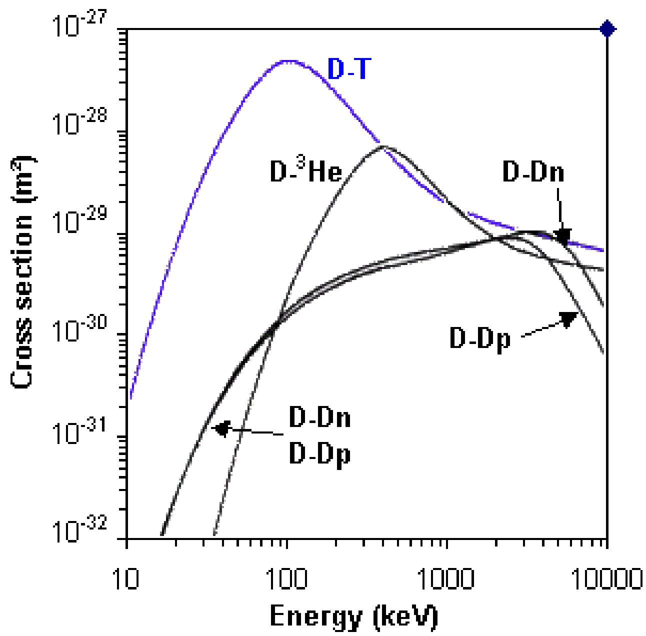

Figure 1.1: Cross section is relevant to the probability that the fusion reaction in given energy interval occurs. For lower energies and thus nuclei temperatures, the cross section of DT reaction is much higher than for other reactions.

(with temperature T in Kelvin). So-called collective behavior takes place in case that $N_D \ggg 1$ fulfills.

There are several thermonuclear reactions. For power plant usage, the reaction has to be strongly exoenergetic with big cross section under relatively mild temperatures. Such a reaction needs also a sufficient energetic gain from one reaction. The best reaction from these points of view is a reaction of deuterium D and tritium T, i.e. a heavy water nucleus and hydrogen isotope with two additional neurons in nucleus. Energetic gain is 98000kWhg^{-1}. See for comparison the cross section as a function of the temperature on the Fig.1.1.

DT reaction goes as

$$D + T \rightarrow^4 He(3.52\text{MeV}) + n(14.1\text{MeV}).$$

Helium and neutron gain in a sum total kinetic energy of 17.62MeV. Realize that tritium is low energy beta emitter with half-life 12 years and is dangerous with regard to internal contamination. For both practical and security reason, it will be profitable to gather the tritium directly in a reactor as a product of nuclear reactions:

$$^6Li + n \rightarrow {}^4He + T + 4.86\text{MeV}$$

$$^7Li + n \rightarrow {}^4He + T + n - 2.5\text{MeV}.$$

In a long time outlook, the fusion reaction on power plants could be on the basis of DD reactions as follows:

$$D + D \rightarrow T\,(1.01\text{MeV}) + p\,(3.3\text{MeV})$$

$$D + D \rightarrow^3 He\,(0.82\text{MeV}) + n\,(2.45\text{MeV}).$$

These reactions require much higher temperatures to take place. Energy profitable is an usage of fusion only in case that the power released from fusion reaction is exceeding the external power needed for plasma heating. The ration of fusion power and external source power is denoted as Q. Sustainable burning (so-called ignition), when plasma is kept in fusion temperatures itself refers to $Q \simeq \infty$. Up to now, no fusion experiment even reached value $Q = 1$, which is called a breakeven. Note that for ITER, the value of Q is scheduled to be 5. The conditions for breakeven are set by Lawson criterion. For DT reaction in temperature region $10 - 20$keV it is

$$nT\tau \approx 6 \cdot 10^{21} m^{-3} \text{keV s},$$

where n is a number of fuel particles in 1m^3, τ is a energy confinement time and T is a temperature in region $10 - 20$keV. The Lawson criterion reveals two main options for breakeven achievement.

Magnetic confinement

An idea is to use strong magnetic fields to reach long particle confinement time under small plasma density (typically $\tau \sim 1$s, $n \sim 10^{20}\text{m}^{-3}$). The longer particle confinement the higher probability that the particle fuse together with another one. The specific configuration of magnetic field prevent particles to be in a contact with vessel wall. Such approach are following reactors like tokamaks or stellarators.

Inertial confinement

It is an opposite case to magnetic confinement. Basic is in extremely fast heating, leading to fusion energy release sooner than the fusing nuclei disperse. It is a non-stationary procedure with typical parameters of $\tau \sim 10^{-11}$s and $n \sim 10^{31}\text{m}^{-3}$. Small pellets with a fuel (DT mixture) is exposed to as symmetric as possible high energy laser pulse in order to focus the pellet and reach a condition agreeable with Lawson criterion.

All around the world, there are plenty of experiments dealing with both magnetic and inertial confinement concept. No matter which method will be more suitable for future commercial power plant the goal is the same, to overcome as soon as possible the breakeven and maintain in this state as long as possible with positive energy output.

1.2 Tokamaks

At the end of previous part we have seen two approaches to the thermonuclear fusion realization under terrestial conditions. In this part we will be focused to tokamaks, the world present record-holder regarding the Lawson criterion compliance. The logical approach reads as follows. Fusion is possible only under high temperatures. The particle energy needs to reach more than 10keV. With a such high energy, electron travels during one second the distance approx. 60000km. In order to force some particles with such energy to fuse, we need some manner of confinement. The particle with electric charge q and mass m is moving with the velocity $\mathbf{v}$. In the magnetic field $\mathbf{B}$ (simplify and imagine that $\mathbf{B} = (0, 0, B)$), particle's equation of motion reads

$$m\frac{\mathrm{d}\mathbf{v}}{\mathrm{d}\mathbf{t}} = q\mathbf{v} \times \mathbf{B}.$$

The cyclotron frequency of its circular motion is thus

$$\omega_c = \frac{|q|\,B}{m}. \tag{1.3}$$

As a consequence, particle will follow a magnetic field with gyration motion with the radius (Larmor radius)

$$r_L \equiv \frac{v_\perp}{\omega_c} = \frac{mv_\perp}{|q|\,B},$$

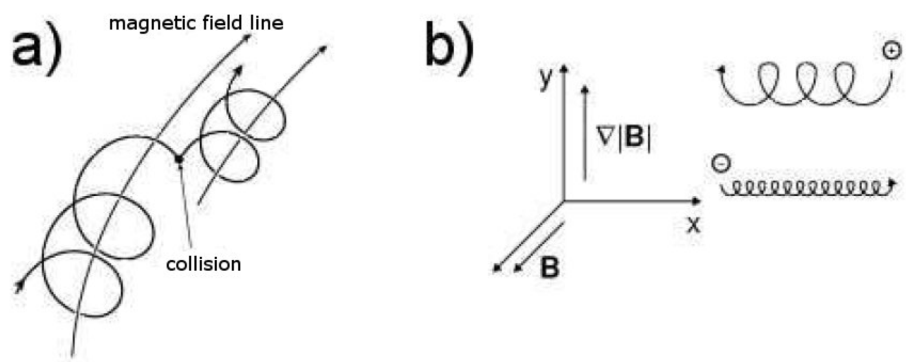

Figure 1.2: Charged particle motion in the presence of a magnetic field. a) motion caused by a collision, b) motion affected by drifts. In this case, it is a gradient of magnetic field drift.

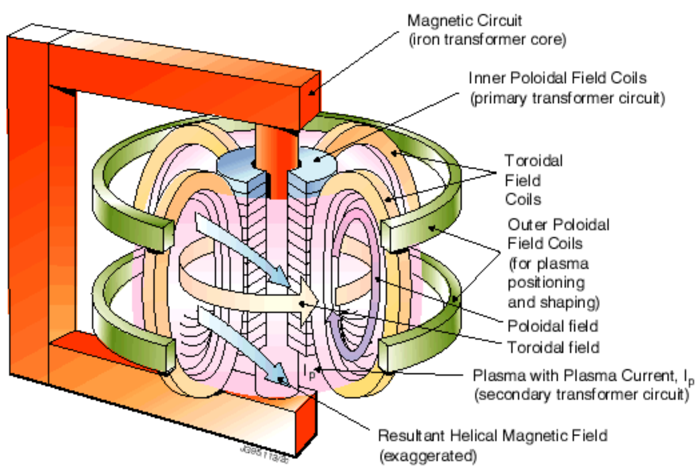

Figure 1.3: Basic tokamak schematic view. The final confinement magnetic field is a sum of a toroidal an poloidal field.

where $v_\perp$is a velocity perpendicular to $\mathbf{B}$. See this motion on the Fig. 1.2. In principle, there are two kinds of magnetic fields present in a tokamak, the toroidal and the poloidal magnetic field. In the poloidal direction placed coils create the basic maintenance toroidal magnetic field. Following these magnetic field lines, charged nuclei and electron follow the above described motion. Nevertheless, these mag. field lines are in a circular shape and this, the centrifugal force appears. This force causes the separation of ions and electrons which creates additional electrical field $\mathbf{E}$. The combination of this electric field and basic toroidal magnetic field cause undesirable drift which affect both electrons and ions in the same way pushing them out of the torus. This drift has a velocity

$$\mathbf{v}_g = \frac{\mathbf{E} \times \mathbf{B}}{B^2}.$$

this phenomenon is called a toroidal drift and has to be mitigated by adding of additional poloidal magnetic field [15]. The combination of toroidal and poloidal magnetic field result in the helical (screwline) magnetic field line (the toroidal field is usually approx. ten times stronger than the poloidal one). See the basic concepts of tokamak on the Fig. 1.3 In this brief tokamak description, we will present only the last aspect, i.e. the plasma heating. Pure ohmic heating is not sufficient. Its maximum value is affected by the tokamak size and by the magnetic field. Ohmic heating is caused by the electric current running the plasma in toroidal direction. It is limited also by the fact that it generates the poloidal magnetic field which can not be arbitrary. Next drawback linked with ohmic heating is the dependence of the electric resistance on the temperature of plasma being $\sim T^{-3/2}$. As a consequence, the more ohmic heating the less effective it is. It is obvious that additional external (I omit now the internal self-heating of plasma fed by fusion products - a helium). heating is demanded. There are two basic possibilities:

NBI - Neutral Beam Injection

The beams of very fast neutral atoms of the fuel (i.e. either D or T) are shot into the plasma. Its velocity is set according to the need in order to inject maximum of its energy into the core plasma. This atoms need to be negative in order to cross the magnetic field surfaces forming the confinement trap for plasma particles. Typical energies of NBI for present tokamak experiments are around 120keV (whereas for ITER, it will reach to 1MeV). One NBI system can feed the plasma with the power around 1MW. Beside heating, it is also an effective tool for plasma refueling and plasma current drive and current and temperature profile shaping.

EM wave heating

Via this method, the eating energy is transferred into the plasma by radiation of electromagnetic waves. Suitable frequencies for plasma heating are close to the cyclotron frequencies of electrons and ions of plasma, i.e. $\omega \approx \omega_c$. For electrons, it is roughly the frequency 28GHz/T per unit of magnetic field. In present tokamaks, it achieves interval of $60-120$GHz. Such waves transfer its energy to electrons which by means of collisions shift the energy to ions, which we seek to heat primary. ion cyclotron resonance frequency is smaller (due to the higher ion mass) and depends on the ion charge and mass. Both frequencies are dependent on the magnetic field which is, in first approximation, dependent on $\sim 1/R$ where R is a main tokamak radius. Practically, there can be used also higher harmonic frequencies. These EM wave heating methods are useful for control and operating of plasma profile, because the high frequency wave energy absorption is a local effect. It allows to eliminate the temperature profile variation and relevant instabilities mitigation.

See broad information in tokamak theory in [21] or in more technology oriented way in [7].

1.3 Electric current in tokamaks

In preliminary concepts of tokamaks, only the transformer effect was used for electric toroidal current generation. It is a fundamental feature of a tokamak, where plasma itself is an only one winding of the secondary transformer loop. Presently, the fact that the transformer effect current generation demands the time change of magnetic flux is a key drawback of this concept, since it is unacceptable for steady state operation. Thus, only during beginning of the plasma discharge is this method used in present experiments. See that the loop voltage U_{LOOP} is defined as

$$U_{LOOP} = -\frac{\mathrm{d}\psi}{\mathrm{d}t},$$

where ψ is a magnetic flux flowing the transformer core. An electric field in the toroidal direction accelerating the plasma particles is after

$$E_T = \frac{U_{LOOP}}{2\pi R}.$$

In case that I_P denotes the total plasma current, the plasma resistivity is in quasistationary regime simply

$$R_P = \frac{U_{LOOP}}{I_P}$$

and ohmic heating power is

$$P_{OH} = U_{LOOP} \cdot I_P.$$

From that we can also see that with temperature increase, the ohmic heating is getting to be less effective.

For longer and advanced tokamak operation modes, the non-inductive current drive is needed. Beside briefly introduced Neutral Beam Injection, there is the LHCD method which will be subject of following paragraph. Less robust tool for external current drive is so-called Bootstrap current being caused by the presence of pressure gradient in the area of trapped particles on specific banana orbits [21]. Further, the radial symmetry of the current profile is gently affected by the Pfirsch-schlueter current. This current is a consequence of the pressure gradient as a result of the Shafranov shift of the magnetic axis.

1.4 LHCD overview

Presently is LHCD installed on all large tokamaks such as Tore Supra, JET, EAST, Alcator C-Mod and will be of course installed on ITER as a part of steady state operation work package. Also on Compass tokamak, there is a schedule for LHCD installation. Lower hybrid waves are quasi-static electric waves propagated in magnetically confined plasmas. These waves may transfer its energy to electrons of plasma by Landau damping [15, 4], leading to acceleration of the electrons motion at the direction along with the wave vector, which is targeted to be the same as a toroidal plasma current. Thus, additional electrical current is driven, that is called LHCD. The high phase velocity or LH waves allows for driving current efficiently and minimizes deleterious effects due to particle trapping. Thus, LHCD has the best efficiency among non-inductive external current drive systems (so-called heating and current drive H&CD systems are NBI, ion cyclotron resonance frequency (ICRH) system, electron cyclotron resonance frequency (ECRH) system and LHCD). It is more effective on lower temperature electrons and thus for off-axis current profile control or for hybrid scenarios. LH waves penetrate better into the plasma at low densities and high magnetic fields. Also, the LHCD assisted start-up reduces flux consumption during current ramp-up phase of plasma discharge, resulting in a longer flat top. In tokamak plasmas, the lower hybrid frequencies are within microwaves [12]. The range of the frequencies is within $\omega_{ci} \ll \omega \ll \omega_{ce}$ (see [10] e.g.). Frequencies as 1.3GHz, 3.7GHz, 4.5GHz or 5GHz (scheduled for ITER) can be considered. This choice is affected by the power supply accessibility, i.e. klystrons. For such high frequencies, the toroidal magnetic field curvature can be neglected. Also the phase velocity is bellow the electron thermal velocity and as a consequence, the LH antenna - plasma coupling s well as the wave propagation can be approximated as a cold plasma problem.

LHCD tool ought to be divided into several steps, launching of the waves via a LH antenna, a grill structure if waveguides placed side by side close to the plasma edge. Further the coupling of the power with the edge plasma, propagation within plasma until the place of absorption by means of Landau damping.

The propagation of LH waves is under above discussed conditions detailed in [13]. General overview is in[10]. Lets define the refraction index as a parallel and perpendicular refraction index:

$$\mathbf{n}_{\parallel} = \left(\mathbf{n} \cdot \frac{\mathbf{B_0}}{B_0}\right) \frac{\mathbf{B_0}}{B_0} \quad \mathbf{n}_{\perp} = \mathbf{n} - \mathbf{n}_{\parallel}, \tag{1.4}$$

where $\mathbf{B_0}$ is a toroidal magnetic field. The wave propagation in plasma is derived from dispersion relation

$$\mathbf{n} \times (\mathbf{n} \times \mathbf{E}) + \overleftrightarrow{\epsilon} \cdot \mathbf{E} = \mathbf{0},$$

where $\overleftrightarrow{\epsilon}$ is a permittivity tensor equal under $+i\omega t$ convention to

$$\overleftrightarrow{\varepsilon} = \epsilon_0 \begin{pmatrix} S & iD & 0 \\ -iD & S & 0 \\ 0 & 0 & P \end{pmatrix}, \tag{1.5}$$

where

$$P = 1 - \frac{\omega_{pe}^2 + \omega_{pi}^2}{\omega^2}$$

$$S = \frac{1}{2}(R + L)$$

$$D = \frac{1}{2}(R - L)$$

$$R = 1 - \frac{\omega_{pe}^2}{\omega(\omega - \omega_{ce})} - \frac{\omega_{pi}^2}{\omega(\omega + \omega_{ci})}$$

$$L = 1 - \frac{\omega_{pe}^2}{\omega(\omega + \omega_{ce})} - \frac{\omega_{pi}^2}{\omega(\omega - \omega_{ci})}.$$

The wave propagation follows this equation:

$$n_\perp^2 = \frac{1}{2S}\left[-\left[n_\parallel^2(P+S) - RL - PS\right]^2 \pm \sqrt{\left[n_\parallel^2(P+S) - RL - PS\right]^2 - 4PS\left(n_\parallel^4 - 2Sn_\parallel^2 + RL\right)}\right]. \tag{1.6}$$

In 2.42, a sign " + " replies to so-called extraordinary (or slow) wave, whereas the sign " − " describes the propagation of so-called ordinary (or fast) wave. In LHCD applications, we take an advantage of a sow wave, which electric field is in the parallel direction with respect to $\mathbf{B_0}$ (as is derived in [13]), as desired for Landau damping effect. Another key drawback of fast wave brand is the fact that its cutoff critical density n_c is a function of magnetic field, more precisely it satisfies an expression

$$e^2 n_c/\epsilon_0 m_e = \omega\omega_{ce}\left(n_\parallel^2 - 1\right)$$

and as a consequence, the evanescent region for fast wave can trench far from the plasma edge, which is unacceptable. In the contrary, for slow wave, the cutoff density reads

$$n_c = \omega^2 \epsilon_0 m_e / e^2.$$

For densities below (i.e. for $f = 3.7\text{GHz}$ it is $n_c = 1.69 \cdot 10^{17}\text{m}^{-3}$) this value, the wave is exponentially damped. The evanescent length is typically several centimeter.

As far as the process of energy transfer from slow wave to the plasma particles is concerned, the kinetic theory has to be introduced. Lets only state that it is because the fundamental of this collisionless wave damping stands on the local reshaping of the fast tail of the velocity distribution function. The resonance condition for damping is

$$\omega - k_\parallel v_\parallel = l\omega_c,$$

where the value of $l = 0$ is the case of Landau damping. There is only few electrons, which are accelerated, but this leads nevertheless to the significant increasing of the toroidal plasma current. I refer for more about Landau damping to [9, 15] e.g.

When speaking about accessibility of the waves, one means the condition giving the limitation for waves to propagate far enough inside the plasma. Accessible is only the region where the slow and fast branch in 2.42 is separated. At the position where the slow and fast wave solution coalesce, the accessibility condition is violated. The energy of slow wave is transferred back to the plasma edge carried by the fast wave. See some examples in [13]. To avoid such situation, the determinant of 2.42 must be positive. It means $n_\perp^2 > 0$. That means the waves with $n_\parallel < 1$ can not propagate to the region of higher densities. The second condition [2, 10, 19, 22] reads

$$n_\parallel^2 > n_{\parallel critical}^2 = 1 + \frac{\omega_{pe}^2}{\omega_{ce}^2}. \tag{1.7}$$

Unfortunately, $n_\parallel^2$ should be as small as possible due to the fact that the CD efficiency is going as $1/n_\parallel^2$. Lets finish this paragraph stating hat the LH antenna has to be placed very near to the plasma edge to decrease effect of evanescent region.

Next aspect is the LH power coupling, which is closely linked to the reflection coefficient of the launching structure, i.e. the LH antenna. This issue is also one of the HAMAC code tasks, to be the tool for antenna design optimization in terms of mitigation of reflection coefficient. Good power coupling avoids undesirable reflected power to the klystrons, which is even more important in present klystrons designs which feed the LH antennas with CW (continual wave) power. Inside the launcher structure, the reflected power can lead to the growth of the electric field which may lead to breakdown. LH waves, which satisfies the accessibility condition 2.7, are launched with an asymmetric parallel wavenumber spectrum. Such waves launcher are made of multiple toroidal arrays of waveguides stacked in one or more poloidal layers, and are commonly named “grill”[1]. The ALOHA code is based on the linear theory [3, 6]. The theory of the LH power coupling is detailed in [9, 16]

1.5 LHCD systems examples

In this part, I would like to give only short brief introduction examples of LHCD systems running on Tore Supra tokamak, where is nowadays headquarters of the development both experimentally and theoretically of LHCD 5GHz system for ITER. Further, I give short overview of LH antenna on EAST tokamak, on which the HAMAC code validation was performed. Last, brief introduction is presented of COMPASS tokamak LH system preview.

1.5.1 LHCD system on Tore Supra

Tore Supra is a French tokamak operated in Cadarache by CEA IRFM. It is present the largest tokamak in the European Union after JET. Unlike JET, Tore Supra has a superconducting toroidal magnets. Therefore, together with the active water cooling of the entire wall and LHCD systems, Tore Supra can operate in very long pulses. Main parameters are: major radius $R_0 = 2.25$m, minor radius $a = 0.7$m, toroidal magnetic field on axis $B_o = 4.5$T, plasma current $I_P = 1.7$MA and pulse length (inductive only) 30sec. Main objectives are non-inductive current generation and continuous heat and particles removal.

In last years, two LHCD antennas were under operation, C2 and C3. Within CIMES project (Tore Supra Composants d’Injection de Matière et d’Énergie Stationnaire), the new Passive-active multijunction (PAM) 3.7GHz antenna C4 has been installed in winter 2009. In the first stage, new antenna is fed by 8 old 500kW klystrons. The usage of 8 new 775kW CW klystrons is scheduled to 2011. Basic advantage of the passive-active concept is to better resist the exposure of high heat fluxes from plasma radiation and heavy neutron loads, as expected in ITER-like size tokamaks. This is because in the PAM antenna, the active (fed) waveguides alternate with

[1]More about the design in the following parts

Figure 1.4: Tore Supra interior

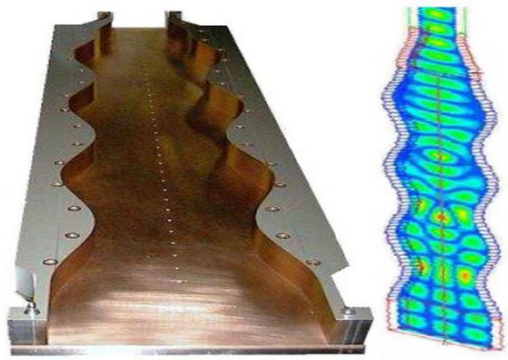

Figure 1.5: Inside of the TE_{10} to TE_{30} mode converter. On the right, RF simulation showing its functionality

the passive $\lambda_g/4$ - deep waveguides (λ_g is a guided wavelength). Behind these passive parts, the free place allows efficient cooling and damping of the neutron energy by a loops of demineralized water steaming through tubes drilled behind the passive waveguides. On the other hand, this scheme reduces the total power radiating surface of the active part. On the contrary, passive waveguides receive part of the reflected power, preventing it to affect the RF generator. After commissioning, 7MW of LHCD power will be available on Tore Supra to drive more than 0.8MA. C3 (fully-active FAM antenna) and also C4 PAM antenna will be fed by 8 CW klystrons.

C3 3.7GHz antenna consists of 6×48 active (about two times more than 128 waveguides in C2 [18]) waveguides and 6×9 passive waveguides. $n_{\parallel}^{peak} \cong 2.02$. The antenna is made of 2 rows of 8 modules, each module contains the TE_{10} to TE_{30} mode converter (see Fig. 1.5). After this converter, module is divided in 3 rows of 6 waveguides. Between each module, there is one passive waveguide.

1.5.2 LHCD system on EAST

Experimental Advanced Superconducting Tokamak (EAST) is the todays only fully superconducting D-shaped divertor plasma configuration tokamak, commissioned in 2006 in the Institut of Plasma Physics of the Chinese Academy of Science (ASIPP), Hefei, China.

The main scientific object is to study the physics and technology of long time advanced steady-state operation and the technology basis of full superconducting (both toroidal and poloidal magnet system) tokamak. The basic EAST parameters reads the magnetic field on axis $B_o =$ 3.5T, plasma current $I_P = 1$MA, major and minor radius $R_0 = 1.7$m, $a = 0.4$m. The maximum pulse long in the first stage is 1000s. Anyhow, the duration of the induced plasma current

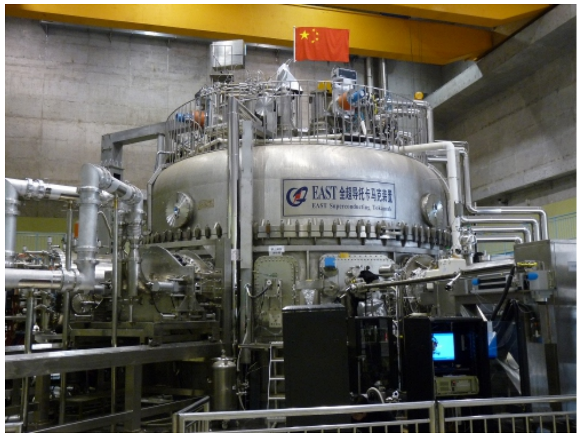

Figure 1.6: Tokamak EAST - general view

by means of the OH transformer is about10s. The in-vessel view of LHCD antenna is on the Fig. 1.7.

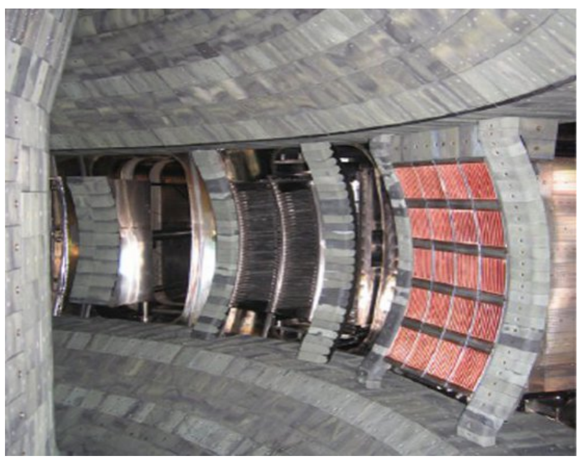

Figure 1.7: EAST in-vessel view with LHCD antenna (right), ICRF antenna (middle) and movable limiter (left) [20]

The geometry is designed for top-bottom symmetry to accommodate both double null and single null divertor configurations. As one can see on the Fig. 1.7, the LHCD grill consists of 5 column times 4 row modules. Each module contains 8 sub-waveguides and is powered by individual klystron (each can deliver CW of 100kW) amplifier. In this thesis, I tested the HAMAC code on the design of one of these 20 identical module. The antenna can launch LHCD power with $n_{\parallel}$ of value $1.6 - 3.2$ with FWHM of 0.2 and $n_{\parallel}^{peak} = 2.3$. The $n_{\parallel}$spectrum can be changed within a fast response time which provides a possible tool for the control of the plasma current density profile. The wave frequency is 2.45GHz. The system will deliver 2MW on EAST tokamak plasma. The big advantage is that the coupling wave spectrum of the system can be gently flexibly adjusted in time.

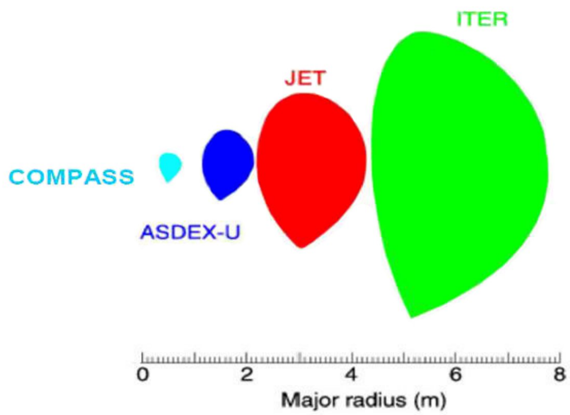

Figure 1.8: Comparison of tokamaks with ITER-like cross section

1.5.3 LHCD system on COMPASS

Tokamak COMPASS (COMPact ASSembly) was originally operated from 1989 in UKAEA, Culham, Great Britain. In 2004, the tokamak was offered for free to the IPP AS CR in Prague, where was successfully reinstalled to generate the first plasma in December 2008. It is the smallest tokamak with a clear H-mode and ITER-like geometry (see Fig. 1.8). In Prague, two flywheel generators of the power 70MW had to be built.

The installation of two new neutral beam injection systems (2×300kW) and LHCD system (3.7GHz, 1MW) is scheduled. Main parameters are: major and minor radius $R_0 = 0.56$m, $a = 0.2$m, magnetic field $0.8 - 2.1$T, plasma current $I_P < 350$kA.

Basic assumption for LHCD system is to use the frequency of 3.7GHz, because the klystrons used will be two Thales Electron Devices TH2103 klystrons being now under replacement in CEA, Cadarache, France. The peak $n_\parallel$ should be within the values 2 and 3 (the propagation of LH waves under this premise in [13]). Finally, the port access to the vacuum vessel is of dimensions 140×170mm. In [18], two antenna designs, meeting all above mentioned constrains, are preliminary mentioned. To estimate the waveguide phasing and width, the following analytical formula (derived in the Annexe 1 of [16]) is used.

$$n_\parallel^{peak} = \frac{\phi_0}{k_0 \Delta}, \tag{1.8}$$

where ϕ_0 is the relative phase between two grill waveguides, k_0 is the wave number in vacuum and Δ is the width of grill waveguide + the width of the septum, separating two neighboring waveguides.

1.6 ALOHA code introduction

In the last part of this chapter, I present the code ALOHA [6, 11]. ALOHA is a MATLAB script with FORTRAN binaries. Its trigger is the aim of improvement of the modeling of the coupling of lower hybrid antenna to a cold inhomogeneous plasma. Before, there problem was catch by linear theory based 1D code SWAN (Slow Wave ANtenna), in which the toroidal lines of waveguides are assumed to be infinite in the poloidal direction. More recently, the code TOPLHA (Torino Politecnico Lower Hybrid Antenna) focus on describing realistic geometries.

It address the problem of LH wave coupling including the toroidal curvature of the plasma as well as the realistic shape of the antenna.

ALOHA itself solves the problem in 2D including both the slow and fast waves. Realistic geometry of antenna is added by full-wave computation. Next advancement with respect to the SWAN is the extending of several layers modeling of the profile of electron density in front of the antenna and thus treat more realistic SOL in front of the antenna. . The resulting reflection coefficients of reference LH antennas on Tore Supra reveals good agreement between the simulation and the measurement made on operating antenna in Tore Supra. One of an important 1D approach consequence is that in case that the grill is composed of more poloidal lines of waveguides, in 1D two waveguides placed one on the other in two different poloidal waveguides line are not coupled by the plasma and the description does not couple these ports.

the antenna coupling is split into two parts, the modeling of the module, the repeatable part of multijunction LH antenna and the modeling of the grill in front of the plasma. At the beginning of the calculus, the HAMAC plug-in (or using the commercial software HFSS) output, i.e. the scattering matrix (lets denote as $[S_{module}]$), quantifying the coupling between the different ports forming LH antenna, is required. After that, the coupling to the plasma of all the waveguides that compose the grill (LH antenna mouth) is desired. The evanescent modes excited at the end of the waveguides are also taken into account. Consequently the scattering matrix of grill/plasma $\left[S_{grill/plasma}\right]$ is derived as a coupling of the grill with the plasma via a surface admittance formulation. Finally, mode matching takes place, i.e. the same modes in both scattering matrices are identified and the global response of the antenna is extracted. See the ALOHA validation, comparison with experimental results and comparison of ALOHA and SWAN and TOPLHA in [11]. Since 2008, the ALOHA code is maintained by Julien Hillaire, CEA, Cadarache in France. Its key utilization is now in a 20MW/5GHz LHCD PAM system which is about to be commissioned and used for the second mission of ITER [8]. The RF analysis of the LH antenna design is performed by, among others, ALOHA. New ITER relevant concept of LHCD multijunction type antenna is now propose, it is a Passive Active Multijunction PAM. It improves the necessary cooling of the neutrons flux in a nuclear environment as needed for ITER while maintaining a good coupling even at large distances from the plasma. Cooling is provided between the columns of waveguides and columns of short passive waveguides, which are short-circuited, between the column of active waveguides. Natural drawback of this concept is the reduction of the radiating surface of the active part of antenna.

Chapter 2

Hybrid Antenna Modeling for the ALOHA Code (HAMAC) description

The aim of the HAMAC code is to calculate the overall scattering matrix of a LH multijunction antenna. The LH multijunction antenna is a phased rectangular waveguide array where the phase shift between two neighbour waveguides is fixed by design. The orientation in the tokamak plasma is such that the electric field vector of TE modes is parallel to the toroidal plasma current. The phasing is resulting in the presence of non zero phase velocity of radiated waves in the toroidal direction. Thus, multijunction antenna embodies the required properties of Landau damping effect, i.e. the electric field in toroidal direction propagation and low reflection which is needed for protecting the klystrons from reflected power, especially when they are working in continuous mode such as on Tore Supra. Next advantage is that the grill avoids any hardware within the plasma chamber, which is about to be a more important in ITER-like size reactors with the significant neutron fluxes. Antenna can be accommodated in one access port of the vessel. LHCD requires that the antenna have an asymmetrical power spectrum in the direction of the toroidal plasma. In some examples of ALOHA code outputs, we will see that it is a case. The main drawback of the multijunction concept is that the mutual waveguide phase shift is fixed by design. Classical approach with no junction of all output waveguides enables free phasing and thus power spectra modification but loose the advantage of mitigation of reflected power which is a case in multijunction concept. An example of the LH multijunction antenna grill is on Fig. 2.1.

The scattering matrix is the basic characteristics of any RF structure which relates the input EM waves ($\overrightarrow{A}$) with the output one ($\overrightarrow{B}$). The scattering matrix coefficients are dimensionless and does not depend on the power applied (the RF device is supposed to be linear). Suppose a RF structure with 3 inputs and 3 outputs (keep in mind that all the time, the number of inputs and outputs is naturally the same) (see Fig. 2.2).

For this example, the scattering matrix reads

$$\begin{pmatrix} B_1 \\ B_2 \\ B_3 \end{pmatrix} = \begin{bmatrix} S_{11} & S_{12} & S_{13} \\ S_{21} & S_{22} & S_{23} \\ S_{31} & S_{32} & S_{33} \end{bmatrix} \begin{pmatrix} A_1 \\ A_2 \\ A_3 \end{pmatrix}. \tag{2.1}$$

Once having the S - matrix of the plasma too, the ALOHA code can calculate the matching of

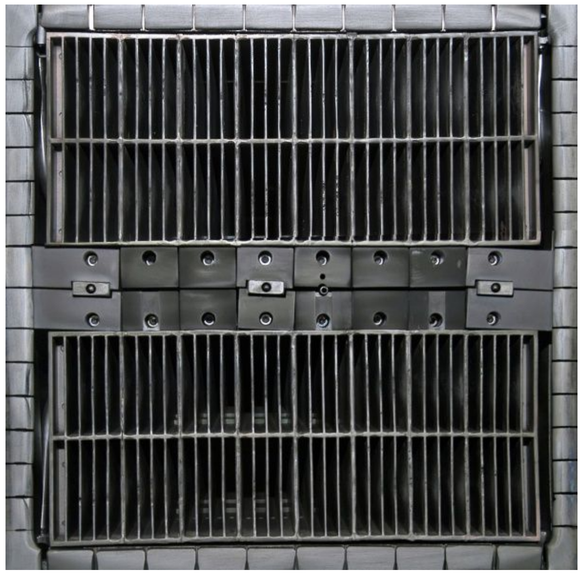

Figure 2.1: An example of frontal view to the LH multijunction antenna grill.

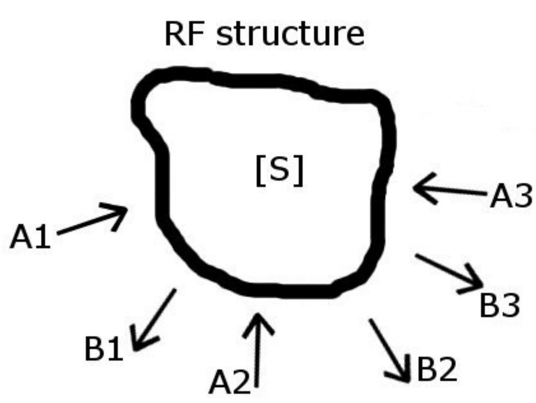

Figure 2.2: A sketch of the general RF structure with several inputs (A) and outputs (B)

this S - matrix with the calculated scattering matrix of the antenna to get the final S - matrix of antenna + plasma $[S]_{A+P}$, which contains the information about the reflected power, since $\mathbf{R} = [S]_{A+P}\,\mathbf{F}$, where$|\mathbf{F}|^2$ is the incident power and $|\mathbf{R}|^2$ is the reflected power. This is a nature of the scattering matrix, it characterizes a RF structure using incident and reflective waves in a ports and not magnetic and electric fields. The waves are only described by the electromagnetic power they carry and a phase, which is contained in imaginary part of all scattering matrix elements.

This chapter will provide full description of HAMAC code calculation. In order to present the S - matrix calculation method, we stress that the multijunction antenna can be in simple case split into separate straight waveguides which are properly plugged one to each other in order to create structures which shift a phase of wave, cause the phase delay or split the incoming power into several outputs in desired ratio of power distribution.This is a reason for the following description. First I present the wave propagation description in the straight waveguide. This can be done either via the TE or the TM mode. With this knowledge we are able to understand the form of S - matrix of the straight waveguide. Further, the S - matrix calculus of the 2D area of two straight waveguide intersection is issued. There are two options. This intersection can be realized either via the waveguide discontinuity or via the junction, i.e. the splitting of one waveguide to more output waveguides. Both cases are discussed since both occur in all the LH antennas. Knowing the S - matrices of all the LH antenna parts, we can proceed the mode-matching technique overarching the whole LH antenna in order to give only one S - matrix describing the whole structure. This matrices cascading is depicted in the last part of this chapter.

2.1 Straight waveguide description

The waveguide is more general term than we will work with in HAMAC for LHCD application. Nevertheless, the original meaning is a hollow conductive metal pipe used to carry high frequency radio waves, particularly microwaves, which is our case. Waveguides are used for low-loss transmission of the EM power. According to the waveguide general design, there are three types of propagation. The transmission lines that consist of two or more conductors can propagate so-called TEM (Transverse ElectroMagnetic) waves, which does not contain longitudinal field components. On the contrary, waveguides for LH applications are made of hollow tubes and can propagate only TE waves (Transverse Electric waves, the electric field is transverse to the direction of the propagation, i.e. $E_x = 0$) and TM waves (Transverse Magnetic waves, the magnetic field is transverse to the direction of the propagation, i.e. $H_x = 0$). The Cartesian coordinates are defined according to the layout in the Fig. 2.3, where parameter "a" is the large side of the rectangular cross-section and the parameter "b" is the small side.

The meaning of the orientation of TE and TM modes on waveguide gives the sketch on the Fig. 2.4. To start the propagation description, we need the presumption of source-free waveguide and the time convention choice of the propagation for example $+j\omega t$. Now, we can say that the propagation follows the maxwell's equations

$$\nabla \times \mathbf{E} = -i\omega\mu\mathbf{H}$$

$$\nabla \times \mathbf{H} = i\omega\epsilon\mathbf{E}.$$

In [?, 17], the evaluation is done to find the expression of electric and magnetic transverse field in the form of the infinite superposition of TE and TM modes:

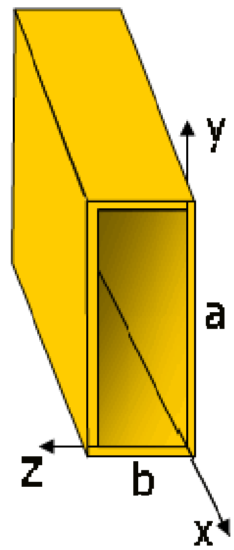

Figure 2.3: HAMAC Cartesian coordinates system of the rectangular waveguide. For an antenna in front of the plasma, x direction refers to the radial direction, y to the poloidal direction and finally z is the direction of the toroidal magnetic field.

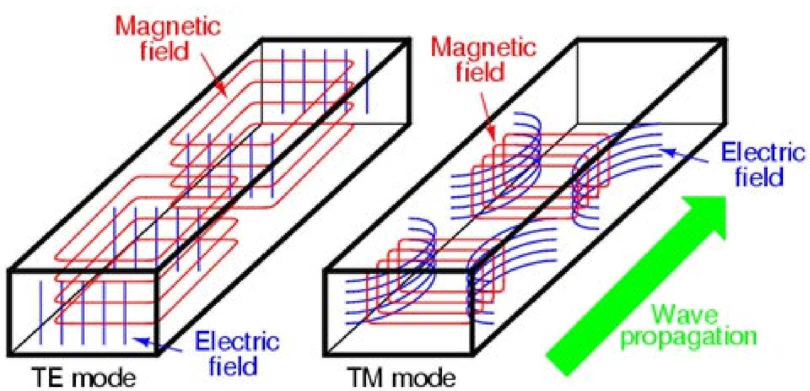

Figure 2.4: With respect to the wave propagation direction, the difference between TE and TM modes is presented in terms of the orientation of electric and magnetic field with respect to the wave propagation.

$$
\begin{aligned}
\mathbf{E}_t(x,y,z) &= \sum_{m,n}\left(A^{TE}_{m,n}\,e^{-ik^{TE}_{g,m,n}x}+B^{TE}_{m,n}\,e^{ik^{TE}_{g,m,n}x}\right)\mathbf{e}^{TE}_{m,n}(y,z)\sqrt{Z^{TE}_{m,n}}\\
&\quad+\sum_{m',n'}\left(A^{TM}_{m',n'}\,e^{-ik^{TM}_{g,m',n'}x}+B^{TM}_{m',n'}\,e^{ik^{TM}_{g,m',n'}x}\right)\mathbf{e}^{TM}_{m',n'}(y,z)\sqrt{Z^{TM}_{m',n'}}\\
\mathbf{H}_t(x,y,z) &= \sum_{m,n}\left(A^{TE}_{m,n}\,e^{-ik^{TE}_{g,m,n}x}-B^{TE}_{m,n}\,e^{ik^{TE}_{g,m,n}x}\right)\mathbf{h}^{TE}_{m,n}(y,z)\sqrt{Y^{TE}_{m,n}}\\
&\quad+\sum_{m',n'}\left(A^{TM}_{m',n'}\,e^{-ik^{TM}_{g,m',n'}x}-B^{TM}_{m',n'}\,e^{ik^{TM}_{g,m',n'}x}\right)\mathbf{h}^{TM}_{m',n'}(y,z)\sqrt{Y^{TM}_{m',n'}},
\end{aligned}
\tag{2.2}
$$

where

- $\mathbf{E}_t$ is the transverse electric field
- $\mathbf{H}_t$ is the transverse magnetic field
- $A^{TE}_{m,n}$ is the complex amplitude of incident wave for $TE_{m,n}$ mode
- $B^{TE}_{m,n}$ is the complex amplitude of reflected wave for $TE_{m,n}$ mode
- $\mathbf{e}^{TE}_{m,n}$ is the electric field eigenvector for $TE_{m,n}$ mode
- $\mathbf{h}^{TE}_{m,n}$ is the magnetic field eigenvector for $TE_{m,n}$ mode
- $Z_{m,n}$ is the characteristic impedance of the mode m,n, defined as
  - $Z^{TE}_{m,n} = Z_0 k_0 / k^{TE}_{g,m,n}$ for TE mode
  - $Z^{TM}_{m,n} = Z_0 k^{TM}_{g,m',n'}/k_0$ for TM mode
  - $Z_0 = \sqrt{\mu_0/\epsilon_0} \simeq 120\pi$ is the impedance of free space
- $Y_{m,n}$ is the characteristic admittance of the mode m,n, defined as $Y_{m,n} = 1/Z_{M,n}$.
- $k_{g,m,n}$ is the guided wavenumber of the mode m,n, where
  - $k_{g,m,n} = \left(k_0^2 - k_{c,m,n}^2\right)^{1/2}$
  - k_0 is the wavenumber in free space
  - $k_{c,m,n}$ is the cutoff wavenumber defined as $k_{c,m,n} = 2\pi/\lambda_c$ with $\lambda_c = 2\frac{\sqrt{ab}}{\sqrt{m^2 b/a + n^2 a/b}}$ where a and b is the height and width of the waveguide.

The coordinate system is the same as in the Fig. 2.3. Both fields are spread into the sum of incident and reflected waves and further into both TE and TM parts. The form of the electric and magnetic eigenvectors for TE and TM is following.

2.1.1 TE and TM modes

On the Fig. 2.4, we see in the reality only the example of modes. As we will see in this part, the TE mode i.e. can have both transverse component according to the small index m, n is 3.2. What stands for TE mode is that the longitudinal component for $\mathbf{E}$ is zero, while the longitudinal component H_x of magnetic field reads [17]

$$H_x(x, y, z) = A_{m,n} \cos \frac{m\pi y}{a} \cos \frac{n\pi z}{b} e^{-i\beta x}, \tag{2.3}$$

where $A_{m,n}$ is an arbitrary amplitude, $m = 0, 1, 2...$, $n = 0, 1, 2...$, β is the propagation constant

$$\beta = \sqrt{k^2 - k_c^2} = \sqrt{k^2 - \left(\frac{m\pi}{a}\right)^2 - \left(\frac{n\pi}{b}\right)^2}, \tag{2.4}$$

where k_c is the cutoff wave number. Thanks our time convention of propagation, the space propagation in x direction follows $-j\beta x$. The propagation constant 3.6 gives the limitation to the modes which will be able to propagate, i.e. which will keep β positive. If it is not a case, the wavenumber β is pure imaginary, which means that all field components will decay exponentially away from the source of excitation. Such modes are called the evanescent modes. Thus we can state that the propagating modes are these with the cutoff wavenumber k_c below vacuum wave number k.

$$k > k_c = \sqrt{\left(\frac{m\pi}{a}\right)^2 + \left(\frac{n\pi}{b}\right)^2}. \tag{2.5}$$

In the contrary, for give shape of the rectangular waveguide (i.e. the dimensions a and b) and for the given environment (characterized by μ and ϵ), we can for given mode set by value of integers m, n find the cutoff frequency as

$$f_{c_{m,n}} = \frac{1}{2\pi\sqrt{\mu\varepsilon}} \sqrt{\left(\frac{m\pi}{a}\right)^2 + \left(\frac{n\pi}{b}\right)^2}. \tag{2.6}$$

The transverse eigenvectors of TE of electric and magnetic fields is [1]

$$\mathbf{e}_{m,n}(y,z) = \begin{pmatrix} e_x \\ e_y \\ e_z \end{pmatrix} = \begin{pmatrix} \textit{not transverse} \\ \frac{\sqrt{\epsilon_m \epsilon_n}}{b} \frac{n}{\sqrt{m^2\, b/a + n^2\, a/b}} \cos\left(\frac{m\pi}{a} y\right) \sin\left(\frac{n\pi}{b} z\right) \\ -\frac{\sqrt{\epsilon_m \epsilon_n}}{a} \frac{m}{\sqrt{m^2\, b/a + n^2\, a/b}} \sin\left(\frac{m\pi}{a} y\right) \cos\left(\frac{n\pi}{b} z\right) \end{pmatrix} \tag{2.7}$$

$$\mathbf{h}_{m,n}(y,z) = \begin{pmatrix} h_x \\ h_y \\ h_z \end{pmatrix} = \begin{pmatrix} \textit{not transverse} \\ \frac{\sqrt{\epsilon_m \epsilon_n}}{a} \frac{m}{\sqrt{m^2\, b/a + n^2\, a/b}} \sin\left(\frac{m\pi}{a} y\right) \cos\left(\frac{n\pi}{b} z\right) \\ \frac{\sqrt{\epsilon_m \epsilon_n}}{b} \frac{n}{\sqrt{m^2\, b/a + n^2\, a/b}} \cos\left(\frac{m\pi}{a} y\right) \sin\left(\frac{n\pi}{b} z\right) \end{pmatrix}, \tag{2.8}$$

where $m, n = 0, 1, 2, 3...$, $\epsilon_m = 1$ for $m = 0$ and $\epsilon_m = 2$ for $m \neq 0$, $\epsilon_n = 1$ for $n = 0$ and $\epsilon_n = 2$ for $n \neq 0$, a is the height of the waveguide in the y direction, b is the width of the waveguide in the z direction. In 2.7 we can now see that the $\mathbf{E}$ field on the Fig. 2.4 refers to case with $n = 0$, i.e. the e_y is in all case zero. The mode with the lowest cutoff frequency, i.e. the mode which should propagate (if nor this mode can propagate then no mode) is called the fundamental mode. The choice $m = 0$, $n = 0$ is not a case because it gives us no nonzero component and thus no propagation. If $a > b$, the fundamental mode for TE has $m = 1,\ n = 0$ and its cutoff frequency is

$$f_{c_{10}} = \frac{1}{2a\sqrt{\mu\epsilon}}. \tag{2.9}$$

For propagation frequency f, all modes with $f_{c_{m,n}} > f$ will not propagate and are called evanescent modes.

Similar formulation as 2.73.6 states for TM modes, for which the transverse eigenvectors in 2.2 are

$$\mathbf{e}_{m,n}(y,z) = \begin{pmatrix} e_x \\ e_y \\ e_z \end{pmatrix} = \begin{pmatrix} \textit{not transverse} \\ -\frac{2}{a}\frac{m}{\sqrt{m^2\,b/a+n^2\,a/b}}\cos\left(\frac{m\pi}{a}y\right)\sin\left(\frac{n\pi}{b}z\right) \\ -\frac{2}{b}\frac{n}{\sqrt{m^2\,b/a+n^2\,a/b}}\sin\left(\frac{m\pi}{a}y\right)\cos\left(\frac{n\pi}{b}z\right) \end{pmatrix} \tag{2.10}$$

$$\mathbf{h}_{m,n}(y,z) = \begin{pmatrix} h_x \\ h_y \\ h_z \end{pmatrix} = \begin{pmatrix} \textit{not transverse} \\ \frac{2}{b}\frac{n}{\sqrt{m^2\,b/a+n^2\,a/b}}\sin\left(\frac{m\pi}{a}y\right)\cos\left(\frac{n\pi}{b}z\right) \\ -\frac{2}{a}\frac{m}{\sqrt{m^2\,b/a+n^2\,a/b}}\cos\left(\frac{m\pi}{a}y\right)\sin\left(\frac{n\pi}{b}z\right) \end{pmatrix}. \tag{2.11}$$

with the same notation as in 2.73.6. Notice that for TM modes, all field components in 2.2 are identically equal zero if either m or n is zero. As a result, the lowest, i.e. the fundamental mode, is TM_{11} mode, having a cutoff frequency

$$f_{c_{11}} = \frac{1}{2\pi\sqrt{\mu\epsilon}}\sqrt{(\pi/a)^2 + (\pi/b)^2}. \tag{2.12}$$

Compare 2.42 and 3.4 to see that $f_{TM_{11}}$ is always higher than $f_{TE_{10}}$. Usually, the waveguides are designed for desired propagation frequency the way that only TE_{10} mode can propagate and all the others, including TM_{11} fundamental mode, are evanescent. We will see in this thesis that it is not the reason for exclusion of these modes in the propagation and S - matrix calculus.

2.1.2 Mode determination

It is not the set of numbers m, n what we are concerned about, but the cutoff frequencies for given mode. Consequently, in HAMAC code, there is not the option to choose the modes to calculate with, but only the total number of modes in each straight waveguide we want to calculate with. The reason is that for give shape of waveguide, the mode $TE_{4,0}$ has much higher cutoff wavenumber than mode $TE_{1,1}$. This is a reason why also not only modes $TE_{m,0}$, as was done in preliminary version of HAMAC [18] is not acceptable choice. Finally, we only determine in code the number of modes and it is automatically chosen the m, n integers with the lowest cutoff frequencies for given μ, ε, a and b. Lets make it clear on the example. We imagine the waveguide with the height of $a = 0.076$m and a width $b = 0.034$m. In the table 2.1 are listed the first 10 modes (both TE and TM) and its cutoff wavenumbers. Modes are sorted on cut-off wavenumbers (i.e. on cut-off frequencies).

We are still not able to say what modes will propagate and what not. This depends on the carrier frequency we force to propagate through the waveguide. For the wave carrier frequency $f = 3.7$GHz, the wavenumber $k_0 = 2\pi\, n\, f/c$ (suppose the index of refraction equal to 1) is equal to $k_0 = 77.5463\text{m}^{-1}$. In table 2.1 we can see that in this case only the TE_{10} will propagate. On the contrary, the frequency $f = 5$GHz could propagate ($k_0 = 104.79\text{m}^{-1}$) all these modes: TE_{10}, TE_{20}, TE_{01}, TE_{11} and TM_{11}.

TE modes									
mode	1 0	2 0	0 1	1 1	2 1	3 0	3 1	4 0	0 2
$k_c[\mathrm{m}^{-1}]$	41.34	82.67	92.40	101.22	123.99	124.01	154.68	165.35	184.79
TM modes									
mode	1 1	2 1	3 1	1 2	4 1	2 2	3 2	5 1	4 2
$k_c[\mathrm{m}^{-1}]$	101.22	123.99	154.68	189.37	189.41	202.45	222.55	226.40	247.97

Table 2.1: An example of the mode selection. For given waveguide cross-section ($a = 0.076$m and $b = 0.034$m) the modes are listed according their cutoff wavenumber.

2.1.3 Orthogonality relations

Further in the calculation description, we will refer to the orthogonality relations between eigenvectors. For no abundance I turn over to [5]with derivation and only write the orthogonality conditions valid for the transverse components as

$$\begin{aligned}
&\iint_s \mathbf{e}_{m,n}^{TE} \otimes \mathbf{h}_{m',n'}^{TE} ds = \delta_{mn,m'n'} \qquad &&\iint_s \mathbf{e}_{m,n}^{TM} \otimes \mathbf{h}_{m',n'}^{TM} ds = \delta_{mn,m'n'} \\
&\iint_s \mathbf{e}_{m,n}^{TE} \otimes \mathbf{h}_{m',n'}^{TM} ds = 0 \qquad &&\iint_s \mathbf{e}_{m,n}^{TM} \otimes \mathbf{h}_{m',n'}^{TE} ds = 0,
\end{aligned} \tag{2.13}$$

where the integration takes place over the transverse section of the guide and

- $\mathbf{e}_{m,n}^{TE}$ is the electric field eigenvector for $TE_{m,n}$ mode
- $\mathbf{h}_{m,n}^{TE}$ is the magnetic field eigenvector for $TE_{m,n}$ mode
- $\mathbf{e}_{m,n}^{TM}$ is the electric field eigenvector for $TM_{m,n}$ mode
- $\mathbf{h}_{m,n}^{TM}$ is the magnetic field eigenvector for $TM_{m,n}$ mode
- $\delta_{mn,m'n'} = \begin{cases} 1 \text{ if } m,n = m',n' \\ 0 \text{ if } m,n \neq m',n' \end{cases}$.

2.2 Separate scattering matrix calculation

At the beginning of this chapter we presented the meaning of S - matrix as well as the idea of how LH antenna looks like. This is the fragmentation of LH antenna into basic straight waveguides, which could be after mutually connected one to each other. We distinguish two kinds of such connection. One is the discontinuity, i.e. either waveguide border reduction or waveguide border enlargement. The second case is the junction, i.e. the connection of one waveguide with more than one other with arbitrary rectangular shape. The example of all mentioned cases can be seen on Fig. 2.5. In following, we will describe how to calculate the S - matrix of a simple straight waveguide. Further, the S - matrix of the discontinuity and junction[1] planes is presented.

[1] I do not specify the kind and the number of the waveguides to be connected

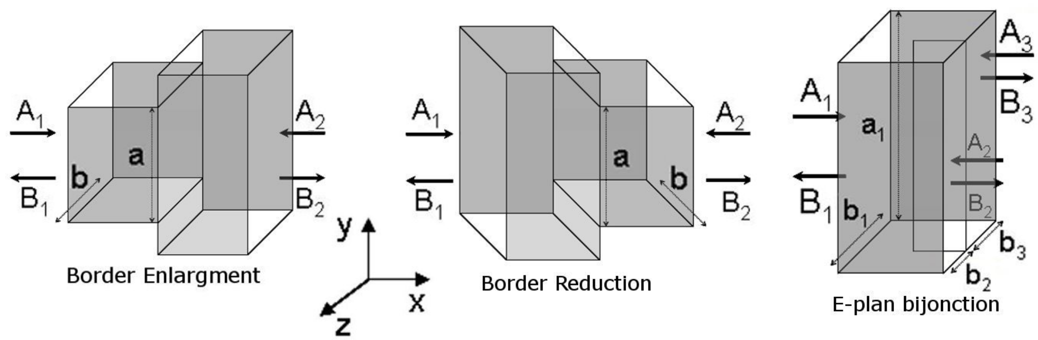

Figure 2.5: An example of possible assembling of the straight waveguides. The wave propagation is in x direction. In all three examples are indicated the inputs (A) and the outputs (B). There is no constrain in the discontinuity type: also the discontinuity in the z direction can take place.

2.2.1 Straight waveguide

Unlike to discontinuity and junction, the S - matrix of a straight waveguide is quite simple. Important to realize that in contradistinction to discontinuity and junction, this is a case of 3D object. In fact, discontinuity and junction is dealing only with 2D area where two straight waveguides touch. We consider here perfect conducting waveguide walls, i.e. the conduction losses can be neglected. This assumption imply that no reflected power is created inside a straight waveguide. In other words, all power entering the waveguide in one end is observed as an output on the other side. Herein I would like to stress that the elements in the S - matrix are the complex numbers. In the case of straight waveguide, the amplitude of the S_{11} and S_{22}, corresponding to return losses, has to be equal to 0. Thus, the form of the S - matrix is as follows

$$\begin{pmatrix} B_1 \\ B_2 \end{pmatrix} = \begin{bmatrix} 0 & D \\ D & 0 \end{bmatrix} \begin{pmatrix} A_1 \\ A_2 \end{pmatrix}, \tag{2.14}$$

where

$$D = \begin{bmatrix} \mathrm{diag}(\exp(-ik^{TE}_{g,m,n} L_x))_{modes} & 0 \\ 0 & \mathrm{diag}(\exp(-ik^{TM}_{g,m,n} L_x))_{modes} \end{bmatrix},$$

with

- $\mathrm{diag}()_{modes}$ is the diagonal matrix. The size is equal to the number of modes taken into account.
- $k^{TE}_{g,m,n}$ is the guided wavenumber of the mode $TE_{m,n}$
- $k^{TM}_{g,m,n}$ is the guided wavenumber of the mode $TM_{m,n}$
- L_x is the length of the straight waveguide

As a consequence, the input and output complex amplitudes in 2.42 reads the form

$$B_1 = \begin{pmatrix} B_1^{TE} \\ \\ B_1^{TM} \end{pmatrix}; \quad B_1^{TE} = \begin{pmatrix} B_1^{TE_{m_1,n_1}} \\ \\ B_1^{TE_{m_2,n_2}} \\ \\ \vdots \\ \\ B_1^{TE_{m_q,n_q}} \end{pmatrix}; \quad B_1^{TM} = \begin{pmatrix} B_1^{TM_{m_1,n_1}} \\ \\ B_1^{TM_{m_2,n_2}} \\ \\ \vdots \\ \\ B_1^{TM_{m_p,n_p}} \end{pmatrix} \tag{2.15}$$

and similarly for B_2, A_1 and A_2. In 3.1, we consider that the output B_1 is in fact the set of different q modes TE and different p modes TM. Note that while cascading two S - matrices, the total number of modes taken into account in both S - matrices has to be equal. Moreover, the matching can take place only between the same modes, i.e. the mode TE_{10} in the first S - matrix has to be present also in the second S - matrix to be matched. See more about the mode selection in previous section.

2.2.2 Discontinuity

As it can be seen on the Fig. 2.5, there is not big difference between BE and BR discontinuity in case we realize that it is only the 2D plate what matters. For S - matrix calculus what change is only the meaning of what input and output A, resp. B is. Thus, in HAMAC code, only the BE discontinuity is implemented. All the time when BR discontinuity is required, only transformation to BE occurs and the same algorithm runs.

The algorithm core used is the modal method assuming the continuity of the transverse electromagnetic field in x direction (passing through the waveguides). The base is in writing the electromagnetic field in the both sides of the discontinuity, i.e. the equations 2.2 (with additional index labeling the side of the discontinuity). WE take an advantage of the freedom in placing the origin of the coordinate x and place it to the position of the discontinuity. Than, the equations 2.2 reads for electric field

$$\begin{aligned}\sum_{m,n} \left(A^{TE}_{1,m,n} + B^{TE}_{1,m,n}\right) \mathbf{e}^{TE}_{1,m,n}(y,z)\sqrt{Z^{TE}_{1,m,n}} + \sum_{m',n'} \left(A^{TM}_{1,m',n'} + B^{TM}_{1,m',n'}\right) \mathbf{e}^{TM}_{1,m',n'}(y,z)\sqrt{Z^{TM}_{1,m',n'}} = \\ \sum_{m,n} \left(A^{TE}_{2,m,n} + B^{TE}_{2,m,n}\right) \mathbf{e}^{TE}_{2,m,n}(y,z)\sqrt{Z^{TE}_{2,m,n}} + \sum_{m',n'} \left(A^{TM}_{2,m',n'} + B^{TM}_{2,m',n'}\right) \mathbf{e}^{TM}_{2,m',n'}(y,z)\sqrt{Z^{TM}_{2,m',n'}}\end{aligned} \tag{2.16}$$

and for magnetic field

$$\begin{aligned}\sum_{m,n} \left(A^{TE}_{1,m,n} - B^{TE}_{1m,n}\right) \mathbf{h}^{TE}_{1,m,n}(y,z)\sqrt{Y^{TE}_{1,m,n}} + \sum_{m',n'} \left(A^{TM}_{1,m',n'} - B^{TM}_{1,m',n'}\right) \mathbf{h}^{TM}_{1,m',n'}(y,z)\sqrt{Y^{TM}_{1,m',n'}} = \\ \sum_{m,n} \left(-A^{TE}_{2,m,n} + B^{TE}_{2,m,n}\right) \mathbf{h}^{TE}_{2,m,n}(y,z)\sqrt{Y^{TE}_{2,m,n}} + \sum_{m',n'} \left(-A^{TM}_{2,m',n'} + B^{TM}_{2,m',n'}\right) \mathbf{h}^{TM}_{2,m',n'}(y,z)\sqrt{Y^{TM}_{2,m',n'}}.\end{aligned} \tag{2.17}$$

The meaning of all indexes and symbols is the same as in 2.2. Now we will use the orthogonality relations 2.13. First lets define for well-arrangement the parameters denoting the different coupling regimes between $TE - TE$, $TE - TM$, $TM - TE$ or $TM - TM$ modes:

$$
\begin{aligned}
R_{hh} &= \iint_s \mathbf{e}_1^{TE} \otimes \mathbf{h}_2^{TE} ds \qquad & R_{he} &= \iint_s \mathbf{e}_1^{TM} \otimes \mathbf{h}_2^{TE} ds \\
R_{eh} &= \iint_s \mathbf{e}_1^{TE} \otimes \mathbf{h}_2^{TM} ds \qquad & R_{ee} &= \iint_s \mathbf{e}_1^{TM} \otimes \mathbf{h}_2^{TM} ds,
\end{aligned}
\tag{2.18}
$$

where the integration is over the contact surface s being the area where both waveguides forming the discontinuity interfere. For simplicity I omit indexing of the modes. Multiply eq. 3.2 from right site with $\otimes \mathbf{h}_2^{TE}$ and integrate over surface s to obtain

$$
R_{hh}\sqrt{Z_1^{TE}}\left(A_1^{TE}+B_1^{TE}\right)+R_{he}\sqrt{Z_1^{TM}}\left(A_1^{TM}+B_1^{TM}\right)=\sqrt{Z_2^{TE}}\left(A_2^{TE}+B_2^{TE}\right). \tag{2.19}
$$

Repeating this procedure by multiplying with $\otimes \mathbf{h}_2^{TM}$ we get

$$
R_{eh}\sqrt{Z_1^{TE}}\left(A_1^{TE}+B_1^{TE}\right)+R_{ee}\sqrt{Z_1^{TM}}\left(A_1^{TM}+B_1^{TM}\right)=\sqrt{Z_2^{TM}}\left(A_2^{TM}+B_2^{TM}\right). \tag{2.20}
$$

Similarly, we get from 2.17 by multiplying by $\mathbf{e}_1^{TE}\otimes$ or $\mathbf{e}_1^{TM}\otimes$ (and of course after integration over s and usage of orthogonality 2.13) following:

$$
\begin{aligned}
\sqrt{Y_1^{TE}}\left(A_1^{TE}-B_1^{TE}\right) &= H_{hh}\sqrt{Y_2^{TE}}\left(A_2^{TE}-B_2^{TE}\right)+H_{eh}\sqrt{Y_2^{TM}}\left(A_2^{TM}-B_2^{TM}\right) \\
\sqrt{Y_1^{TM}}\left(A_1^{TM}-B_1^{TM}\right) &= H_{he}\sqrt{Y_2^{TE}}\left(-A_2^{TE}+B_2^{TE}\right)+H_{ee}\sqrt{Y_2^{TM}}\left(-A_2^{TM}+B_2^{TM}\right),
\end{aligned}
\tag{2.21}
$$

where

$$
\begin{aligned}
H_{hh} &= \iint_s \mathbf{e}_1^{TE} \otimes \mathbf{h}_2^{TE} ds \qquad & H_{he} &= \iint_s \mathbf{e}_1^{TE} \otimes \mathbf{h}_2^{TM} ds \\
H_{eh} &= \iint_s \mathbf{e}_1^{TM} \otimes \mathbf{h}_2^{TE} ds \qquad & H_{ee} &= \iint_s \mathbf{e}_1^{TM} \otimes \mathbf{h}_2^{TM} ds.
\end{aligned}
\tag{2.22}
$$

We are now able to put all the eq. 2.42, 3.1, 3.2 together by defining following block matrices:

$$
R=\begin{bmatrix}
\sqrt{Z_2^{TE}}^{-1}R_{hh}\sqrt{Z_1^{TE}} & \sqrt{Z_2^{TE}}^{-1}R_{he}\sqrt{Z_1^{TM}} \\
\sqrt{Z_2^{TM}}^{-1}R_{eh}\sqrt{Z_1^{TE}} & \sqrt{Z_2^{TM}}^{-1}R_{ee}\sqrt{Z_1^{TM}}
\end{bmatrix} \tag{2.23}
$$

$$
H=\begin{bmatrix}
\sqrt{Y_1^{TE}}^{-1}H_{hh}\sqrt{Y_2^{TE}} & \sqrt{Y_1^{TE}}^{-1}H_{he}\sqrt{Y_2^{TM}} \\
\sqrt{Y_1^{TM}}^{-1}H_{eh}\sqrt{Y_2^{TE}} & \sqrt{Y_1^{TM}}^{-1}H_{ee}\sqrt{Y_2^{TM}}
\end{bmatrix}. \tag{2.24}
$$

See the definition of parameters 2.18, 3.4 to find that the R matrix in 3.6 and H matrix in 2.42are transposed and thus,

$$H = {}^{t}R,$$

where ^{t} is the transposition operator. With block matrices R and H, we can simply 2.42, 3.1, 3.2 into compact block formula

$$\begin{aligned} R\,(A_1 + B_1) &= (A_2 + B_2) \\ (A_1 - B_1) &= -H\,(A_2 - B_2)\,, \end{aligned} \tag{2.25}$$

where A_1, A_2, B_1 ad B_2 is in the form of 2.15. An algebraic modification gives us from previous equations 3.1 the final expression of S - matrix:

$$\begin{pmatrix} B_1 \\ B_2 \end{pmatrix} = [S] \begin{pmatrix} A_1 \\ A_2 \end{pmatrix} = \begin{bmatrix} S_{11} & S_{12} \\ S_{21} & S_{22} \end{bmatrix} \begin{pmatrix} A_1 \\ A_2 \end{pmatrix}, \tag{2.26}$$

where is

$$\begin{aligned} S_{11} &= [I_1 + HR]^{-1}\,[I_1 - HR] \\ S_{12} &= 2\,[I_1 + HR]^{-1}\,H \\ S_{21} &= R\,[S_{11} + I_1] \\ S_{22} &= RS_{12} - I_2, \end{aligned}$$

and I_1 and I_2 are identical matrices of the dimensions equal to the sum of TE and TM modes in the first, resp. in the second waveguide forming BE discontinuity.

All we have to know are the integrals 2.18 and 3.4. Since I omitted to write index m, n, we have to keep in mind that for example integral R_{hh} is in fact the matrix with all the m, n modes considered. The parameter R_{hh} represents the coupling between TE modes at the first part of the discontinuity and TE modes at the second part. Similarly for other parameters in 2.18 and 3.4. I present only analytical solution of R_{hh}, the others have the similar structure and result. The form is as follows:

$$R_{hh} = \xi_1\, I_1\, I_2 + \xi_2\, I_3\, I_4, \tag{2.27}$$

where

$$\begin{aligned} \xi_1 &= \frac{\sqrt{\epsilon_{m_1}\epsilon_{n_1}}}{b_1} \frac{n_1}{\sqrt{m_1^2\, b_1/a_1 + n_1^2\, a_1/b_1}} \cdot \frac{\sqrt{\epsilon_{m_2}\epsilon_{n_2}}}{b_2} \frac{n_2}{\sqrt{m_2^2\, b_2/a_2 + n_2^2\, a_2/b_2}} \\ \xi_2 &= \frac{\sqrt{\epsilon_{m_1}\epsilon_{n_1}}}{a_1} \frac{m_1}{\sqrt{m_1^2\, b_1/a_1 + n_1^2\, a_1/b_1}} \cdot \frac{\sqrt{\epsilon_{m_2}\epsilon_{n_2}}}{a_2} \frac{m_2}{\sqrt{m_2^2\, b_2/a_2 + n_2^2\, a_2/b_2}}, \end{aligned} \tag{2.28}$$

where $m, n = 0, 1, 2, 3...$, $\epsilon_m = 1$ for $m = 0$ and $\epsilon_m = 2$ for $m \neq 0$, $\epsilon_n = 1$ for $n = 0$ and $\epsilon_n = 2$ for $n \neq 0$, a is the height of the waveguide in the y direction, b is the width of the waveguide in the z direction. Added to this, there are indexes 1 and 2 telling the one site of discontinuity (guide 1) and the second (guide 2) apart. The meaning of parameters I_1, I_2, I_3, I_4 in 3.4 is

$$
\begin{aligned}
I_1 &= \frac{1}{2\pi}\left\{\frac{1}{\underset{-}{n}}\left[\sin\left(\pi\underset{-}{n}(d_b+b_1)-\frac{n_1}{b_1}\pi d_b\right)-\sin\left(\pi\underset{-}{n}d_b-\frac{n_1}{b_1}\pi d_b\right)\right]\right. \\
&\quad -\frac{1}{\underset{+}{n}}\left[\sin\left(\pi\underset{+}{n}(d_b+b_1)-\frac{n_1}{b_1}\pi d_b\right)-\sin\left(\pi\underset{+}{n}d_b-\frac{n_1}{b_1}\pi d_b\right)\right] \\
I_2 &= \frac{1}{2\pi}\left\{\frac{1}{\underset{-}{m}}\left[\sin\left(\pi\underset{-}{m}(d_a+a_1)-\frac{m_1}{a_1}\pi d_a\right)-\sin\left(\pi\underset{-}{m}d_a-\frac{m_1}{a_1}\pi d_a\right)\right]\right. \\
&\quad +\frac{1}{\underset{+}{m}}\left[\sin\left(\pi\underset{+}{m}(d_a+a_1)-\frac{m_1}{a_1}\pi d_a\right)-\sin\left(\pi\underset{+}{m}d_a-\frac{m_1}{a_1}\pi d_a\right)\right]
\end{aligned}
$$

$$
\begin{aligned}
I_3 &= \frac{1}{2\pi}\left\{\frac{1}{\underset{-}{n}}\left[\sin\left(\pi\underset{-}{n}(d_b+b_1)-\frac{n_1}{b_1}\pi d_b\right)-\sin\left(\pi\underset{-}{n}d_b-\frac{n_1}{b_1}\pi d_b\right)\right]\right. \\
&\quad +\frac{1}{\underset{+}{n}}\left[\sin\left(\pi\underset{+}{n}(d_b+b_1)-\frac{n_1}{b_1}\pi d_b\right)-\sin\left(\pi\underset{+}{n}d_b-\frac{n_1}{b_1}\pi d_b\right)\right] \\
I_4 &= \frac{1}{2\pi}\left\{\frac{1}{\underset{-}{m}}\left[\sin\left(\pi\underset{-}{m}(d_a+a_1)-\frac{m_1}{a_1}\pi d_a\right)-\sin\left(\pi\underset{-}{m}d_a-\frac{m_1}{a_1}\pi d_a\right)\right]\right. \\
&\quad -\frac{1}{\underset{+}{m}}\left[\sin\left(\pi\underset{+}{m}(d_a+a_1)-\frac{m_1}{a_1}\pi d_a\right)-\sin\left(\pi\underset{+}{m}d_a-\frac{m_1}{a_1}\pi d_a\right)\right]
\end{aligned}
$$

where

$$
\begin{aligned}
\underset{-}{n} &= \frac{n_1}{b_1}-\frac{n_2}{b_2} \qquad & \underset{+}{n} &= \frac{n_1}{b_1}+\frac{n_2}{b_2} \\
\underset{-}{m} &= \frac{m_1}{a_1}-\frac{m_2}{a_2} \qquad & \underset{+}{m} &= \frac{m_1}{a_1}+\frac{m_2}{a_2}
\end{aligned}
\tag{2.29}
$$

and d_a and d_b is the relative shift of the guide 2 with respect to the guide 1 in y, resp. z direction. See the Fig. 2.6 where the example of relative shifts d_a and d_b is depicted.

As a conclusion of this paragraph, to calculate the S - matrix of the BE discontinuity, 2D plane between waveguide 1 and waveguide 2, one has to know:

- a_1, the high of the first waveguide
- b_1, the width of the first waveguide
- a_2, the high of the second waveguide
- b_2, the width of the second waveguide
- d_a, the relative shift of the second waveguide with respect to the first one, in y direction
- d_b, the relative shift of the second waveguide with respect to the first one, in z direction

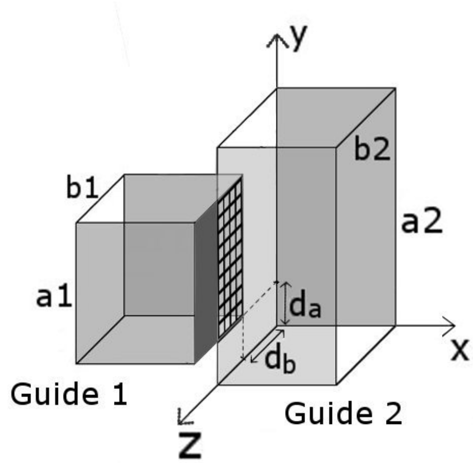

Figure 2.6: Definition of the relative shift d_a and d_b. This values can be also negative. The crosshatched part is referring to the mutual area s, over which the integration in 2.18 and 2.22 takes place.

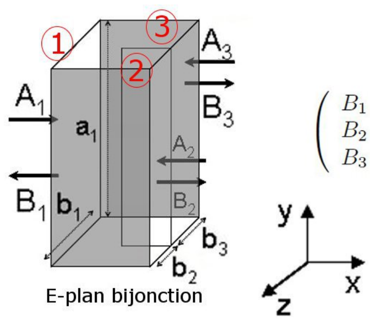

$$\begin{pmatrix} B_1 \\ B_2 \\ B_3 \end{pmatrix} = \begin{pmatrix} S_{11} & S_{12} & S_{13} \\ S_{21} & S_{22} & S_{23} \\ S_{31} & S_{32} & S_{33} \end{pmatrix} \begin{pmatrix} A_1 \\ A_2 \\ A_3 \end{pmatrix}$$

Figure 2.7: The E-plane bi-junction. On the right side, the expected form of the S - matrix. Note that while speaking about *junction*, we talk only about the (y, z) plane with $x = 0$.

- N_M_{TE1}, number of TE modes in the first waveguide (optional)
- N_M_{TM1}, number of TM modes in the first waveguide (optional)
- N_M_{TE2}, number of TE modes in the second waveguide (optional)
- N_M_{TM2}, number of TM modes in the second waveguide (optional)

2.2.3 Junction

At a glance i seems that the junction needs another approach than discontinuity. Contrary is the case. First, we briefly describe the procedure of S - matrix calculation in case of the basic E-plan bi-junction on the Fig. 2.7. After that, we will deal with the general case.

In previous part we experienced BE / BR discontinuity as the 2D plane at the intersection of two guides forming discontinuity. The idea is to use the knowledge of S - matrix of the BE (resp. BR) discontinuity. We can look on the E-plane bi-junction as a system of two BR discontinuities placed side-by-side. On the Fig. 2.7, we can imagine that the HAMAC code goes as:

$$guide\,1 \longmapsto discontinuity\,1\,and\,2 \longmapsto discontinuity\,1\,and\,3 \longmapsto guide\,2 + guide\,3.$$

Following the notation of the guides in the Fig. 2.7 and the meaning of the d_a and d_b parameters, as showed in the Fig. 2.6 (relative shift of two guides), we can say that for specific case on the Fig. 2.7, $d_a^{12} = 0$, $d_b^{12} = b_3 + \triangle$, $d_a^{13} = 0$ and $d_b^{13} = 0$. The superior index marks the case of BR discontinuity between guide 1 and 2, or between guide 1 and 3. Parameter $\triangle$ is a septum (plane separating the guide 2 and guide 3) width. To find the S - matrix of the system on the Fig. 2.7, we can directly adopt the form of block - matrix R, H (2.24, 2.23). We can find two independent sets of equations 3.1[2], one for BR discontinuity between guide 1 and 2 and the other for guide 1 and guide 3. We can write both cases together the way as follows:

$$(A_1 + B_1) = [\ R^{12} \quad R^{13}\ ] \begin{pmatrix} A_2 + B_2 \\ A_3 + B_3 \end{pmatrix} \tag{2.30}$$

$$\begin{bmatrix} H^{12} \\ H^{13} \end{bmatrix} (A_1 - B_1) = \begin{pmatrix} -A_2 + B_2 \\ -A_3 + B_3 \end{pmatrix}. \tag{2.31}$$

We are looking for the solution in the form of

$$\begin{pmatrix} B_1 \\ B_2 \end{pmatrix} = \begin{bmatrix} S_{11} & S_{12} \\ S_{21} & S_{22} \end{bmatrix} \begin{pmatrix} A_1 \\ A_2 \end{pmatrix}. \tag{2.32}$$

Lets define this input and output amplitude vectors:

$$B_{out} = \begin{pmatrix} B_2 \\ B_3 \end{pmatrix}; \quad A_{out} = \begin{pmatrix} A_2 \\ A_3 \end{pmatrix}.$$

With this definition, we can adjust 3.1 and 3.2 We can directly write the resulting S - matrix 3.4 as

$$\begin{pmatrix} B_1 \\ B_{out} \end{pmatrix} = [S] \begin{pmatrix} A_1 \\ A_{out} \end{pmatrix} = \begin{bmatrix} S_{11} & S_{12} \\ S_{21} & S_{out\,out} \end{bmatrix} \begin{pmatrix} A_1 \\ A_{out} \end{pmatrix} \tag{2.33}$$

$$\begin{aligned} S_{out\,out} &= [I_{2+3} + HR]^{-1} [I_{2+3} - HR] \\ S_{21} &= 2\,[I_{2+3} + HR]^{-1} H \\ S_{12} &= R\,[S_{22} + I_{2+3}] \\ S_{11} &= RS_{21} - I_1, \end{aligned}$$

where

- I_{2+3} is the identical matrix of the dimension equal to the sum of TE and TM modes in the guide 2 and guide 3.
- I_1 is the identical matrix of the dimension equal to the sum of TE and TM modes in the guide 1.

[2]See that we need to interchange of index 1 and 2, due to fact that equation 3.1 describes BE discontinuity while we now refer to BR discontinuity.

As previously,under presented formalism is still valid $R = [R^{12} \;\; R^{13}]; \quad H =^t R = \begin{bmatrix} H^{12} \\ H^{13} \end{bmatrix}$.

The equivalent procedure can be applied to the general case when more than 2 guides are on the output of the junction. Also, not only E-plane, but also H-plane[3] junction can be considered. All we have to know are the shifts d_a^{1i} and d_b^{1i} where superior index i denotes the i-th guide forming the junction. The S - matrix coefficients in 3.5 are in this case

$$\begin{aligned} S_{out\,out} &= \left[I_{\sum_i} + HR\right]^{-1} \left[I_{\sum_i} - HR\right] \\ S_{21} &= 2\left[I_{\sum_i} + HR\right]^{-1} H \\ S_{12} &= R\left[S_{22} + I_{\sum_i}\right] \\ S_{11} &= RS_{21} - I_1, \end{aligned} \tag{2.34}$$

with

- $B_{out} = \begin{pmatrix} B_2 \\ B_3 \\ \vdots \\ B_g \end{pmatrix}; \quad A_{out} = \begin{pmatrix} A_2 \\ A_3 \\ \vdots \\ A_g \end{pmatrix}$
- $g - 1$is a number of output guides forming the junction
- $I_{\sum_i}$ is the identical matrix of dimension equal to the sum of TE and TM modes in the guide number $2, 3, ..., g$.
- I_1 is the identical matrix of dimension equal to the sum of TE and TM modes in the guide 1.
- $R = [R^{12} \; R^{13} \; \cdots \; R^{1g}]; \quad H =^t R = \begin{bmatrix} H^{12} \\ H^{13} \\ \vdots \\ H^{1g} \end{bmatrix}$.

2.3 Mode matching - matrices cascading

The HAMAC code first calculate all sub S - matrices, i.e. S - matrices of all straight waveguides discontinuities and junctions. Last task is to match all of them together. we show how to connect them each other in order to obtain the global S - matrix which describes the set of waveguides - LH antenna as a whole. We can never match two S - matrices which do not have the same modes in the sides to be matched. Though, since we do not match two straight waveguides directly together, but indirectly via its discontinuity S - matrix, we have to take care only of keeping the same number of modes on the sides to be matched - the mode itself will be identical, because we match always planes with the same high and width. First, we show how to match two S - matrices, for example the waveguide with BE discontinuity. The graphical representation of this procedure can be seen on Fig. 2.8 (red circle).

In the guide 1, there is the same number of TE and TM modes at the beginning of the guide and at the end (i.e. the size of vector A_1 is the same as vector B_2 and also the size of vector B_1 is equal to the size of vector A_2). Further, there has to be valid following equalities

[3]In this case, the dividing septum is not a slab in (x, y) plane, but in (x, z) plane.

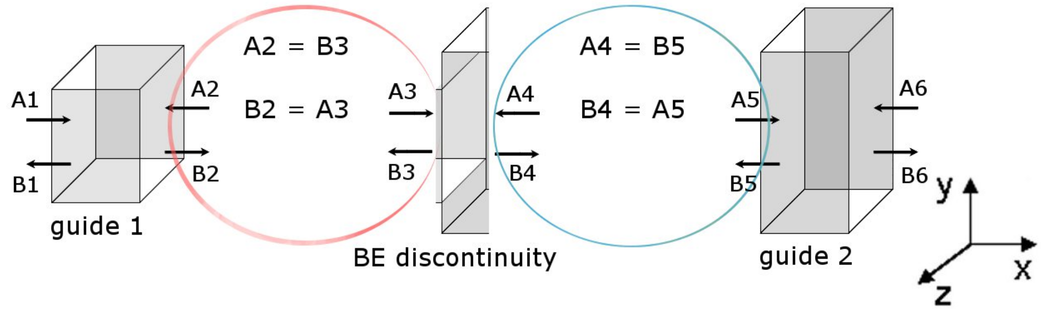

Figure 2.8: The principle of the cascading. Two S - matrices are put together in each step.

$$\begin{aligned} A_2 &= B_3 \\ B_2 &= A_3. \end{aligned} \tag{2.35}$$

It says that the output of guide 1 is exactly what enter the BE discontinuity, i.e. the input A_2. Similarly in opposite direction.

We know that for guide 1 we can write

$$\begin{aligned} B_1 &= S^1_{11}A_1 + S^1_{12}A_2 \\ &B_2 = S^1_{21}A_1 + S^1_{22}A_2 \end{aligned} \tag{2.36}$$

and for BE discontinuity we can write

$$\begin{aligned} B_3 &= S^{BE}_{11}A_3 + S^{BE}_{12}A_4 \\ B_4 &= S^{BE}_{21}A_3 + S^{BE}_{22}A_4. \end{aligned} \tag{2.37}$$

After matrices cascading, we seek for the following global scheme

$$\begin{pmatrix} B_1 \\ B_4 \end{pmatrix} = [S] \begin{pmatrix} A_1 \\ A_4 \end{pmatrix}, \tag{2.38}$$

or

$$\begin{aligned} B_1 &= S^{final}_{11}A_1 + S^{final}_{12}A_4 \\ B_4 &= S^{final}_{21}A_1 + S^{final}_{22}A_4. \end{aligned} \tag{2.39}$$

Since 2.42 is valid, we can solve the system of equations 2.42, 3.1, 3.2, 3.4 to get

$$\begin{aligned} S^{final}_{11} &= S^1_{12}[I - S^{BE}_{11}\,S^1_{22}]^{-1}\,S^{BE}_{11}S^1_{21} + S^1_{11} \\ S^{final}_{12} &= S^1_{12}[I - S^{BE}_{11}\,S^1_{22}]^{-1}\,S^{BE}_{12} \\ S^{final}_{21} &= S^{BE}_{21}[I - S^1_{22}\,S^{BE}_{11}]^{-1}\,S^1_{21} \\ S^{final}_{22} &= S^{BE}_{21}[I - S^1_{22}\,S^{BE}_{11}]^{-1}\,S^1_{22}S^{BE}_{12} + S^{BE}_{22}, \end{aligned} \tag{2.40}$$

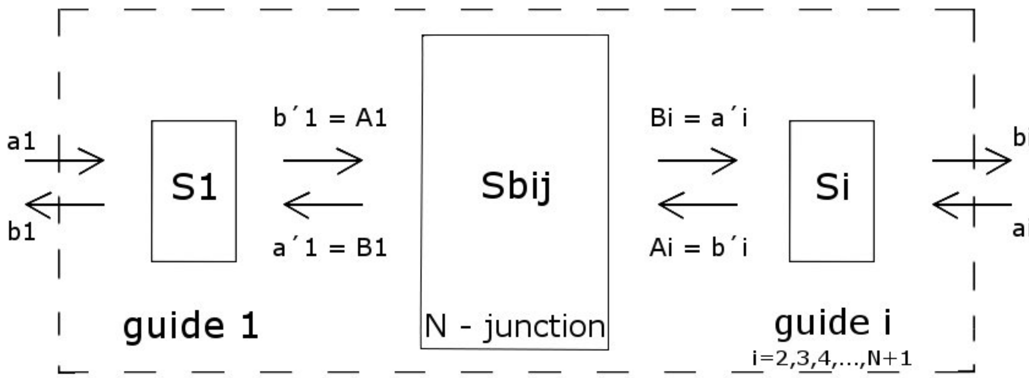

Figure 2.9: Scheme of N-junction cascading. There is one waveguide before junction plane and N waveguides after. These guides are indexed by i. Labels A, a are inputs, B, b are outputs. On the figure are indicated mutual relations between inputs and outputs within multijunction.

where I is the identical matrix of dimension equal to the sum of TE and TM modes in the intersection, i.e. in the end of guide 1 or entrance of BE discontinuity. We can see that all we work with in this part are results of previous S - matrix calculus, where we expected to match all the time only parts with the same number of modes. This is the reason for ensuring that the block matrix $[S]$ in 3.3 has right number of rows and columns as it should have with respect to the size of $\begin{pmatrix} B_1 \\ B_4 \end{pmatrix}$.

2.3.1 Multijunction

In the end of this chapter describing the computation mechanism of HAMAC plug-in, we present the procedure of cascading the structure where after one straight waveguide, the multi junction appears. Generally, there is no restriction on the number of waveguides forming the junction. Suppose we have a N-junction. Total number of waveguides is thus $N+1$. The situation is in the Fig. 2.9.

Consider to know the S - matrix of guide 1 (S^1), N - junction ($S^{N-junction}$) and all output guides ($S^i,\ i \in \{2, 3, ..., N+1\}$).

$$[S^1] = \begin{bmatrix} S^1_{11} & S^1_{12} \\ S^1_{22} & S^1_{21} \end{bmatrix}, \quad [S^{N-junction}] = \begin{bmatrix} S^{N-junction}_{11} & S^{N-junction}_{12} \\ S^{N-junction}_{22} & S^{N-junction}_{21} \end{bmatrix}, \quad [S^i] = \begin{bmatrix} S^i_{11} & S^i_{12} \\ S^i_{22} & S^i_{21} \end{bmatrix}.$$

To do so, we have to know all the dimensions of all straight waveguides and also the relative shifts between guide 1 and other guides. Of course, number of TE and TM modes is also desired. We seek for the analytical form of S^{global} in the following structure:

$$\begin{pmatrix} b_1 \\ b_{out} \end{pmatrix} = [S^{final}] \begin{pmatrix} a_1 \\ a_{out} \end{pmatrix} = \begin{bmatrix} S^{final}_{11} & S^{final}_{12} \\ S^{final}_{22} & S^{final}_{21} \end{bmatrix} \begin{pmatrix} a_1 \\ a_{out} \end{pmatrix}, \tag{2.41}$$

where

$$b_{out} = \begin{pmatrix} b_{i=2} \\ b_{i=3} \\ \vdots \\ b_{i=N+1} \end{pmatrix}; \qquad a_{out} = \begin{pmatrix} a_{i=2} \\ a_{i=3} \\ \vdots \\ a_{i=N+1} \end{pmatrix}$$

Taking into account the equalities $a'_1 = B_1$, $b'_1 = A_1$, $a'_i = B_i$, $b'_i = A_i$ (see Fig. 2.9), we can derive[4] following set of equations

$$\begin{aligned} b_1 &= \left[S^1_{11} + S^1_{12} S^{N-junction}_{11} \varphi^{-1}_{11} S^1_{21}\right] a_1 + \left[-S^1_{12} S^{N-junction}_{11} \varphi^{-1}_{11} \varphi_{12} + S^1_{12} S^{N-junction}_{12}\right] A_{out} \quad (2.42) \\ b_{out} &= S^{out}_{21} S^{N-junction}_{21} \varphi^{-1}_{11} S^1_{21}\, a_1 + \left[-S^{out}_{21} S^{N-junction}_{21} \varphi^{-1}_{11} \varphi_{12} + S^{out}_{12} S^{N-junction}_{22}\right] A_{out} + S^{out}_{22}\, a_{out}, \end{aligned}$$

where

- $S^{out}_{11} = \begin{bmatrix} S^{i=2}_{11} & 0 & \cdots & 0 \\ 0 & S^{i=3}_{11} & \cdots & 0 \\ \vdots & \vdots & \ddots & \vdots \\ 0 & 0 & \cdots & S^{i=N+1}_{11} \end{bmatrix}; \qquad S^{out}_{12} = \begin{bmatrix} S^{i=2}_{12} & 0 & \cdots & 0 \\ 0 & S^{i=3}_{12} & \cdots & 0 \\ \vdots & \vdots & \ddots & \vdots \\ 0 & 0 & \cdots & S^{i=N+1}_{12} \end{bmatrix}$
- $S^{out}_{21} = \begin{bmatrix} S^{i=2}_{21} & 0 & \cdots & 0 \\ 0 & S^{i=3}_{21} & \cdots & 0 \\ \vdots & \vdots & \ddots & \vdots \\ 0 & 0 & \cdots & S^{i=N+1}_{21} \end{bmatrix}; \qquad S^{out}_{22} = \begin{bmatrix} S^{i=2}_{22} & 0 & \cdots & 0 \\ 0 & S^{i=3}_{22} & \cdots & 0 \\ \vdots & \vdots & \ddots & \vdots \\ 0 & 0 & \cdots & S^{i=N+1}_{22} \end{bmatrix}$
- $A_{out} = \left(\varphi_{22} - \varphi_{21}\varphi^{-1}_{11}\varphi_{12}\right)^{-1} \left(S^{out}_{12}\, a_{out} - \varphi_{21}\varphi^{-1}_{11} S^1_{21}\, a_1\right)$

with

- $\varphi_{11} = I_1 - S^1_{22} S^{N-junction}_{11}; \qquad \varphi_{12} = -S^1_{22} S^{N-junction}_{12}$
- $\varphi_{21} = -S^{out}_{11} S^{N-junction}_{21}; \qquad \varphi_{22} = I_{out} - S^1_{11} S^{N-junction}_{22}$
- I_1 is the identical matrix of dimension equal to the sum of TE and TM modes in the guide 1
- I_{out} is the identical matrix of dimension equal to the sum of TE and TM modes at the beginning of guides 2, 3, $\ldots N+1$.

From 2.42, It is possible to derive the form of 3.6. As a result, S^{global} matrix elements are

- $S^{global}_{11} = S^1_{11} + S^1_{12} S^{N-junction}_{11} \varphi^{-1}_{11} S^1_{21} - \left[-S^1_{12} S^{N-junction}_{11} \varphi^{-1}_{11} \varphi_{12} + S^1_{12} S^{N-junction}_{12}\right] \cdot \left[\varphi_{22} - \varphi_{21}\varphi^{-1}_{11}\varphi_{12}\right]^{-1} \varphi_{21}\varphi^{-1}_{11} S^1_{21}$
- $S^{global}_{12} = \left[-S^1_{12} S^{N-junction}_{11} \varphi^{-1}_{11} \varphi_{12} + S^1_{12} S^{N-junction}_{12}\right] \cdot \left[\varphi_{22} - \varphi_{21}\varphi^{-1}_{11}\varphi_{12}\right]^{-1} S^{out}_{12}$
- $S^{global}_{21} = S^{out}_{21} S^{N-junction}_{21} \varphi^{-1}_{11} S^1_{21} - \left[-S^{out}_{21} S^{N-junction}_{21} \varphi^{-1}_{11} \varphi_{12} + S^{out}_{21} S^{N-junction}_{22}\right] \cdot \left[\varphi_{22} - \varphi_{21}\varphi^{-1}_{11}\varphi_{12}\right]^{-1} \varphi_{21}\varphi^{-1}_{11}$
- $S^{global}_{22} = \left[-S^{out}_{21} S^{N-junction}_{21} \varphi^{-1}_{11} \varphi_{12} + S^{out}_{21} S^{N-junction}_{22}\right] \cdot \left[\varphi_{22} - \varphi_{21}\varphi^{-1}_{11}\varphi_{12}\right]^{-1} S^{out}_{12} + S^{out}_{22}$

[4] I present only the result since the derivation is not difficult but extensive.

Chapter 3

HAMAC code results

The main advantage of HAMAC code is the direct intuitive simulation of multijunction module for LH antenna. It contains also several functions serving the purpose of the optimization, mode conversion study or trials design. In the first part of this chapter, we will present as an example the phase shifter design optimization. In following section, we give the objective justification of the need of TM modes presence in the calculus, even if its cutoff frequencies prohibit the propagation in the structure. For several antenna parts, the comparison of the resulting S - matrices for calculation with and without TM modes is presented.

In next, we give brief consideration about the question of the optimal number of TE and TM to be taken into account with respect to the result accuracy versus calculation time. In next part of this chapter, as the matter of HAMAC validation, we present the design and S - matrices of LH antenna operated on the tokamak EAST and its comparison with the commercial HFSS software results. Remind that S - matrix elements are a complex numbers, where we separately study an amplitude and a phase. The consistence of HAMAC code was tested also by checking that the power is conserved. That means the sum $\sum_{i=1}^{N} S_{1i}^2 = 1$, where N is number of RF structure ports (see Fig. 2.2), is valid at all the time. In the end of this part, we discuss the limitations for design trial of planned LH antenna for COMPASS tokamak and based on that, two proposals for the antenna are presented. The mutual phase shifts of antenna is compared between the theory, HFSS software and HAMAC. HAMAC output (i.e. S - matrices) are used in ALOHA code to get the reflection coefficient in dependence on electron edge density.

3.1 Optimization tools

The most used waveguide structure is the phase shifter. With respect to the straight waveguide, transmitting wave has after passing throw the phase shifters changed phase angle. The straight waveguide must have, of course, the same length and cross section as a phase shifter. The simple phase shifter can be made by cascading of three waveguides. Usually, for manufacturing simplicity and modularity reasons, the middle waveguide has less high. Such phase shifter is modeled by cascading of the straight waveguide, BR discontinuity, middle straight waveguide with appropriately smaller cross-section, BE discontinuity of the same parameters as the first one and finally the last straight waveguide. Imagine we have a straight waveguide as defined on the Fig. 3.1 (left part).

In HAMAC, the scan over (by user set) number of different simple phase shifter shapes can be done in order to find the best possible shape in terms of the S_{22} coefficient in the S - matrix.

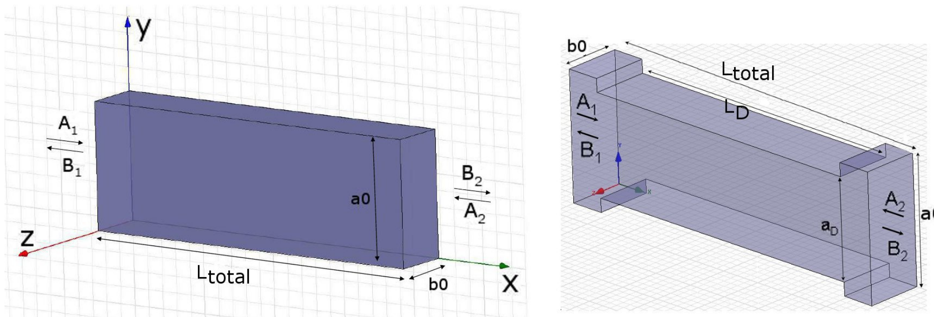

Figure 3.1: On left: straight waveguide example $a_0 = 0.076$m, $b_0 = 0.034$m, $L_{total} = 0.2179$m. On right: an example of simple phase shifter. For different a_D, i.e. the high of middle waveguide and L_D, i.e. the length of middle waveguide, we get different phase shift and different S_{22} (reflection) coefficient. Convenient frequency is 3.7GHz.

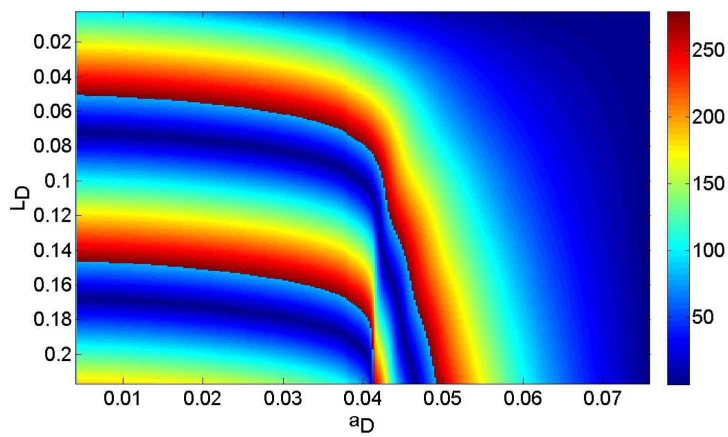

Figure 3.2: The phase shift of simple phase shifter: $a_0 = 0.076$m, $b_0 = b_D = 0.034$m, $L_{total} = 0.2179$m. Propagating frequency is 3.7GHz. Different phase shift (shift with respect to the case of straight waveguide on Fig.3.1) can be seen for several combinations of a_D and L_D.

This coefficient is the reflection coefficient. The aim is to find the shape of phase shifter - middle waveguide (see the right pat of Fig.3.1) for which this S_{22} is as small as possible. According to the degree of freedom we have in the design proposal, different results are possible. The first one (Fig.3.2) shows the different phase shift as a function of a_D, i.e. high of middle waveguide and of L_D, i.e. length of the middle waveguide. Of course, we have to set the other parameters as well as the propagating frequency and number of modes we force to use in the calculus. The second one (Fig.3.3) shows S_{22} coefficients under the same design parameters. .

We seek for as small values of S_{22} as possible in order to ensure the minimum of the power to be reflected (especially at the first discontinuity) back to the entrance into the phase shifter. On Fig.3.3 we can see that for small values of either a_D or L_D, this coefficient is incompetently big - for such design, almost all power will be reflected back in the plane of BR discontinuity. This is expect-able because it corresponds to very big transverse metal plate reflecting the power back. Generally, we see that for low reflection, we need to reduce the high of the middle waveguide just a little. In the contrary, the length of the middle waveguide L_D does influence the reflection in periodical run and reveals more options in the choice. Beside the graphical interpretation,

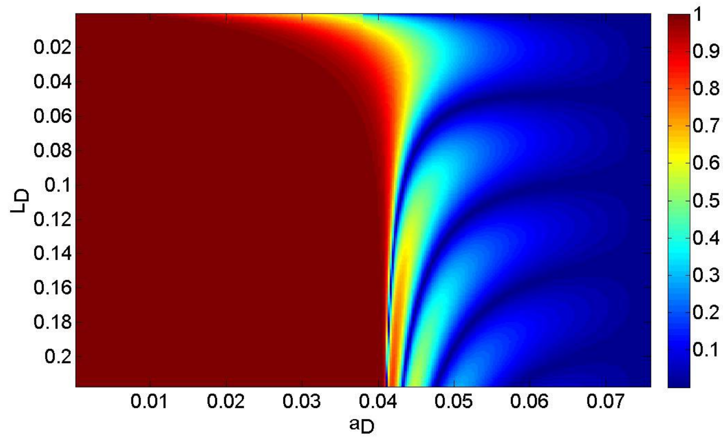

Figure 3.3: S_{22} coefficient for different a_D and L_D, height and length of middle waveguide of the simple phase shifter. Other parameters of the phase shifter are: $a_0 = 0.076$m, $b_0 = 0.034$m, $L_{total} = 0.2179$m. Frequency is 3.7GHz. See Fig.3.1.

we can directly input in the HAMAC the phase shift we want to model and the tolerance of the result. The calculation duration depends on the number of modes we apply and on the number of steps of calculation in x and z direction. In this simulation, we keep the waveguides width constant, as is usual for manufacturing and simplicity reasons in LH antennas. The comparison of the results of cases when we force TM modes and when we omit them gives us important result: since there is no difference, we can say that in the phase shift structures, where the b parameter (waveguides width) does not change, the presence of TM modes brings no importance and thus can be neglected, which accelerate the overall calculation by factor of 2. We will see more about that issue later.

As mentioned above, there are also another optimization tools in HAMAC code, For example, when either a_D or L_D has to be fixed for any reason, scan over other parameters can be done with the similar output as in the example described above. For example, we can imagine the simple phase shifter as on right part of Fig.3.1, i.e. with dimensions $a_0 = 0.076$m, $b_0 = 0.034$m, $L_{total} = 0.2179$m. We want to fix the length of middle waveguide, for a value $L_D = 0.1779$m e.g. In chart 3.4, we can see dependence of phase shift on the high of middle waveguide. For one phase shift value there is more than one dimension choice giving us the possibility to decide according to the corresponding reflection parameter S_{22}.

Thus, the choice of appropriate a_D is unambiguous, since we have to consider the reflection, i.e. term S_{22}. For the same studied phase shifter, i.e. ,$a_0 = 0.076$m, $b_0 = 0.034$m, $L_{total} = 0.2179$m, S_{22} dependence on a_D is in figure 3.5. While deciding the high of middle waveguide for requested phase shift, we have to look at Fig. 3.5 to find the possible result with S_{22} as small as possible.

In order to decrease the S_{22} value more, one can design a so-called double phase shifter[1]. It is kind of phase shifter where two steps of waveguide cross-section change appears. That means first two BR and after two BE discontinuities are present. An example is on Fig. 3.6. In LH antennas, double phase shifters are usually used. These additional steps length are in fact quarter wavelength waveguides, which purpose is to match impedance between waveguides sections and thus minimize the reflected power which may be created by the difference of waveguide height. The dimensions of the double phase shifter on Fig.3.6 are: $a_1 = 0.07$m; $a_2 = 0.061$m; $a_3 =$

[1] Or even more cascaded multi phase shifter. This is, nevertheless, practically not used since the double phase shifter reveals already sufficient mitigation of the reflection parameter S_{22}.

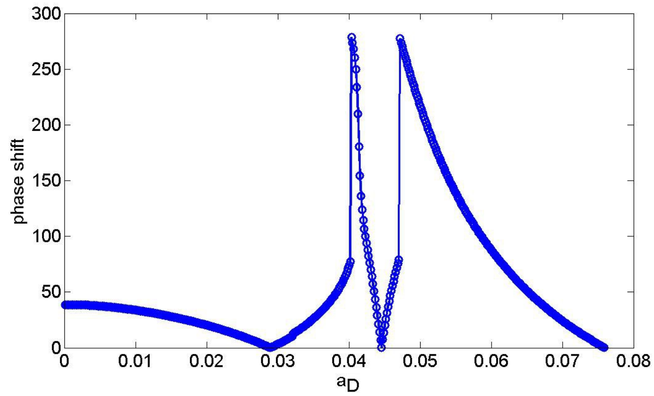

Figure 3.4: Simple phase shifter (right part of Fig.3.1). For fixed length of middle waveguide, the dependence of the phase shift on high of middle waveguide is displayed.

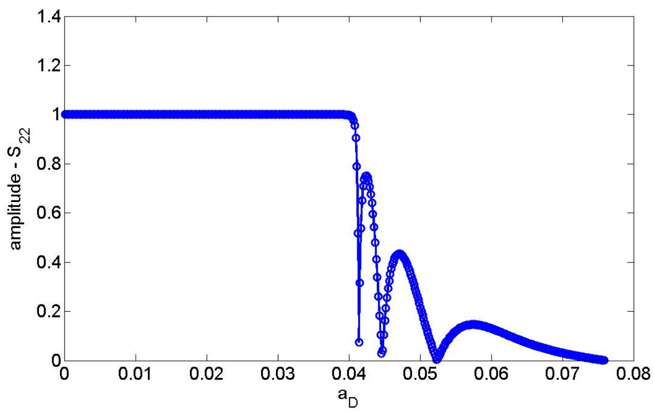

Figure 3.5: Simple phase shifter (right part of Fig.3.1). For fixed length of middle waveguide, the dependence of the S_{22} coefficient on high of middle waveguide is plotted.

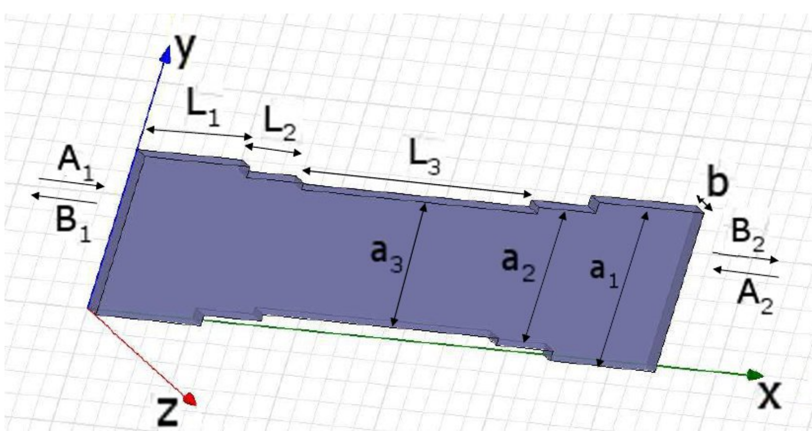

Figure 3.6: An example of double phase shifter. Usually, it has a symmetric structure. The reflection is smaller than in case of simple phase shifter.

0.055m; $b = 0.007$m; $L_1 = 0.05$m; $L_2 = 0.0271$m; $L_3 = 0.1122$m. This is a $-90°$ phase shifter. For a frequency 3.7GHz, we get the S - matrices as follows. We display only the S - matrix coefficients of TE_{10} mode, which is the only propagating one. I modeled the same double phase shifter in HFSS commercial software too. We can compare results obtained by HAMAC with HFSS results. In all the time, we will separate the amplitude and the phase of the complex number of element of S - matrix.

$$
\begin{aligned}
S^{amplitude}_{HAMAC} &= \begin{bmatrix} 0.0127 & 0.9999 \\ 0.9999 & 0.0127 \end{bmatrix}; \qquad S^{amplitude}_{HFSS} = \begin{bmatrix} 0.0131 & 0.9999 \\ 0.9999 & 0.0131 \end{bmatrix} \\
S^{phase}_{HAMAC} &= \begin{bmatrix} 114 & -155 \\ -155 & 114 \end{bmatrix}; \qquad S^{phase}_{HFSS} = \begin{bmatrix} 113 & -154 \\ -154 & 113 \end{bmatrix}.
\end{aligned} \tag{3.1}
$$

We can see that we got a good agreement, since the difference in the amplitude is of order of 10^{-3} and in phase of order of $1°$. The reflection is very small ($10 \cdot \log(0.0127) = -18.9$dB). We can try to fix the maximum outer space ($a = 0.07$m; $b = 0.007$m; $L_{total} = 0.2664$m) and find the equivalent $-90°$ simple phase shifter (frequency stays of course the same, i.e. 3.7GHz). Using the techniques described above, good results give the solution with following parameters:

phase shift	S_{22}	a_D	L_D
-90.14	0.064	0.0569	0.1711

The conclusion is that for this case, the reflection ($S_{22} = 0.064 = -11.9$dB) is higher than for the equivalent double phase shifter. On the other hand, presented solution for simple phase shifter has quite low reflection yet.

3.2 TM modes justification

An important issue during HAMAC code development [18] is the implementation of the TM modes in calculus. This is also key part of present HAMAC version. We learned that TM modes are usually evanescent and one could consider them as a redundant in the light of calculus time consumption. Indeed, the presence of TM modes double the calculation time. We already saw that in case of the straight waveguide there is purely no difference in resulting S - matrix obtained with or without TM in calculation. Now we will make similar test with the structure - E-plane bi-junction. Such bi-junction is in Fig.3.7. On this example, the width of the waveguides change.The simulation of this RF structure was done in HFSS software and also in HAMAC. In HAMAC, I run two times the calculation, first with only $TE_{m,n}$ modes and after also with $TM_{m,n}$ modes. The amplitude and phase of S - matrix, as calculated by HFSS and HAMAC is:

$$
\begin{aligned}
S^{amplitude}_{HFSS} &= \begin{bmatrix} 0.0149 & 0.707 & 0.707 \\ 0.707 & 0.5065 & 0.494 \\ 0.707 & 0.494 & 0.5065 \end{bmatrix} & S^{phase}_{HFSS} &= \begin{bmatrix} 166.36 & -15.95 & -15.95 \\ -15.95 & -48.04 & 131.1 \\ -15.95 & 131.1 & -48.04 \end{bmatrix} \\
\begin{matrix}\text{without}\, TM \\ S^{amplitude}_{HAMAC}\end{matrix} &= \begin{bmatrix} 0.0149 & 0.707 & 0.707 \\ 0.707 & 0.507 & 0.4927 \\ 0.707 & 0.4927 & 0.507 \end{bmatrix} & \begin{matrix}\text{without}\, TM \\ S^{phase}_{HAMAC}\end{matrix} &= \begin{bmatrix} 163.96 & -15.92 & -15.92 \\ -15.92 & 174.46 & -5.83 \\ -15.92 & -5.83 & 174.46 \end{bmatrix} \\
\begin{matrix}\text{with}\, TM \\ S^{amplitude}_{HAMAC}\end{matrix} &= \begin{bmatrix} 0.0149 & 0.707 & 0.707 \\ 0.707 & 0.5066 & 0.4934 \\ 0.707 & 0.4934 & 0.5066 \end{bmatrix} & \begin{matrix}\text{with}\, TM \\ S^{phase}_{HAMAC}\end{matrix} &= \begin{bmatrix} 164.62 & -15.93 & -15.93 \\ -15.93 & -44.13 & 135.07 \\ -15.93 & 135.07 & -44.13 \end{bmatrix}
\end{aligned} \tag{3.2}
$$

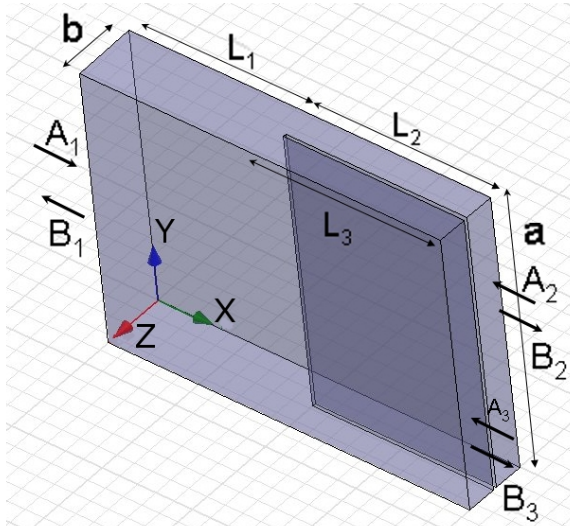

Figure 3.7: An example of E-plane bi-junction. $f = 3.7$GHz; $a = 30.076$m; $b = 0.017$m; $L_1 = L_2 = L_3 = 0.05$m. The septum of thickness 0.5mm is placed in the middle.

To compare the amplitude part of S - matrix, there is a perfect correspondence of the order of 10^{-3}. The number 0.707 in amplitude part of S - matrices means that the power of propagating wave is split equally ($0.707^2 = 0.5$), which was expected since the septum is placed in this model in the middle of bi-junction plane. The design of this bi-junction is very good because there is almost no reflection ($\left(S_{11}^{amplitude}\right)^2 = 0.0149^2 = 2.2 \cdot 10^{-4}$). we see a wrong phase in S_{22}, S_{23} if TM modes are omitted. When TM modes are taken into account, the phase is corresponding to HFSS results with an accuracy of 3°. This means that in the plane of bi-junction, we have to keep TM modes. On the other hand, more important is that the terms S_{12} and S_{13} , resp. S_{21} and S_{31} are equal one to each other. We will see even bigger difference in results without TM modes in following example.

We will also explain what happens in the region of waveguide where discontinuity appears. We will see that TM modes play important role only when b (width) is changed. We present the same test as was done with structure on the Fig. 3.7. Now, the width is changing in two steps. We will compare results HFSS and HAMAC simulation of the RF structure in Fig.3.8. See the resulting amplitude and phase of S - matrix in 3.3

$$\begin{aligned}
S_{HFSS}^{amplitude} &= \begin{bmatrix} 0.449 & 0.893 \\ 0.893 & 0.449 \end{bmatrix} & S_{HFSS}^{phase} &= \begin{bmatrix} 176.06 & -25.55 \\ -25.55 & -47.16 \end{bmatrix} \\
\overset{\text{without}\,TM}{S_{HAMAC}^{amplitude}} &= \begin{bmatrix} 0.420 & 0.908 \\ 0.908 & 0.420 \end{bmatrix} & \overset{\text{without}\,TM}{S_{HAMAC}^{phase}} &= \begin{bmatrix} 156.73 & -10.98 \\ -10.98 & 1.32 \end{bmatrix} \\
\overset{\text{with}\,TM}{S_{HAMAC}^{amplitude}} &= \begin{bmatrix} 0.444 & 0.896 \\ 0.896 & 0.444 \end{bmatrix} & \overset{\text{with}\,TM}{S_{HAMAC}^{phase}} &= \begin{bmatrix} 174.92 & -24.76 \\ -24.76 & -44.44 \end{bmatrix}
\end{aligned} \tag{3.3}$$

Only in case when TM modes are not neglected, we get the corresponding values both for amplitude and for phase. In amplitude, the results obtained by HAMAC are equal to HFSS with error in order of 10^{-3}. Without TM modes, 17.64% of input power is reflected ($0.42^2 = 0,1764$). HFSS and HAMAC with TM modes, nevertheless, says the value of 19.94%. It means that the neglection of TM modes caused some effect mitigation which is important for reflection!

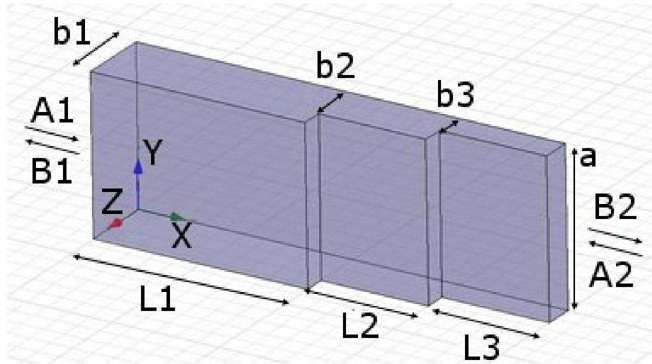

Figure 3.8: E-plane double discontinuity. $a = 0.72$m; $b_1 = 0.034$m; $b_2 = 0.024$m; $b_3 = 0..14m$; $L_1 = 0.1$m; $L_2 = 0.05$m; $L_3 = 0.05$m. Frequency if propagation wave is 3.7GHz.

In phase, the results differ in order of 3°. The difference between results is bigger than in case of E-plane bi-junction. We will see that this is because in the example of bi-junction we presented, the septum thickness is very small (only 0.5mm). Lets see the electric field lines in the area of E-plane discontinuity. The explanation of needfulness of TM modes in the area of E-plane discontinuity is based on the boundary condition on the electric field in the waveguide. It stated that it must be perpendicular at the surface of a conductor. Thus, around the discontinuity, the electric field line needs to have a small component in direction parallel to x-coordinate too (discontinuity is in (y, z) plane). Such orientation must be interpreted as a sum of TE and TM modes. As a result, there are TM modes generated and we should take them into account, while calculating S - matrix of such discontinuity. On the contrary, in H-plane bi-junction, or discontinuity with constant waveguide width, above described problem does no occur. In the example of bi-junction at the beginning of this section (see Fig. 3.7), the problem was only very insignificant since only the width of the septum was responsible for the difference of results in phase of S - matrices.

The width of the metallic area in (y, z) plane (either bi-junction septum or discontinuity plane) influence the range of presence of E field line component in x direction (and of course, also the reflectivity). Thus, the narrower septum the better. This hypothesis is also confirmed by images of electric field line around the plane of first discontinuity of E-plane in Fig. 3.8. In figures 3.9, 3.10, we can see the electric field lines in the area of discontinuity. At each figure, E field at different phase is shown. We can see that around discontinuity plane, vector of E field has component in both x (associated with TM modes) and z (associated with TE modes) direction. These figures also reveal that the effect is only of local nature since further from discontinuity, we can see on 3.9 or 3.10 that the field lines are again without the component in x direction.

3.3 Modes optimization

Since the computation time matters, we tried to find the formula or at least the judgment of what is the sufficient number of modes to consider in order to find the S - matrix with correct values. First, we will study the H-plane discontinuity, i.e. when width in second waveguide is not changed and after, we will deal with E-plane discontinuity, when the height stay constant, but width in second waveguide is changed. As we already demonstrated, in former, only TE modes can be considered, whereas in latter, also TM modes have to be taken into account to meet good correspondence to HFSS results.

Mode testing was performed on the waveguide structure illustrated in Fig. 3.11. First waveguide

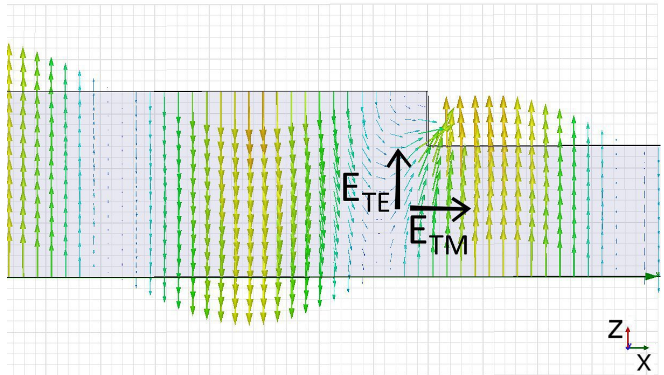

Figure 3.9: E field lines close to the discontinuity. E field has a component in x direction, which means the TM modes are generated, even if they can not propagate further.

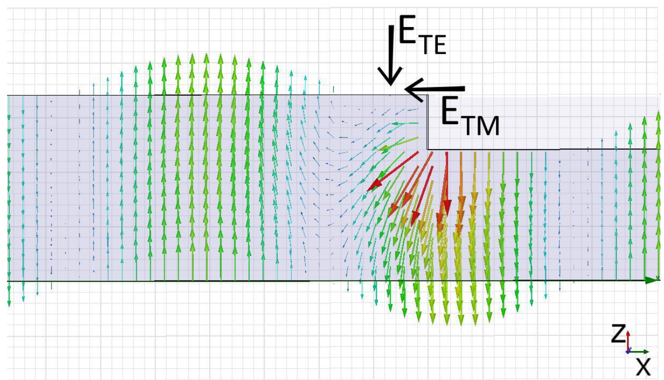

Figure 3.10: E field lines close to the discontinuity. E field has a component in x direction, which means the TM modes are generated, even if they can not propagate further.

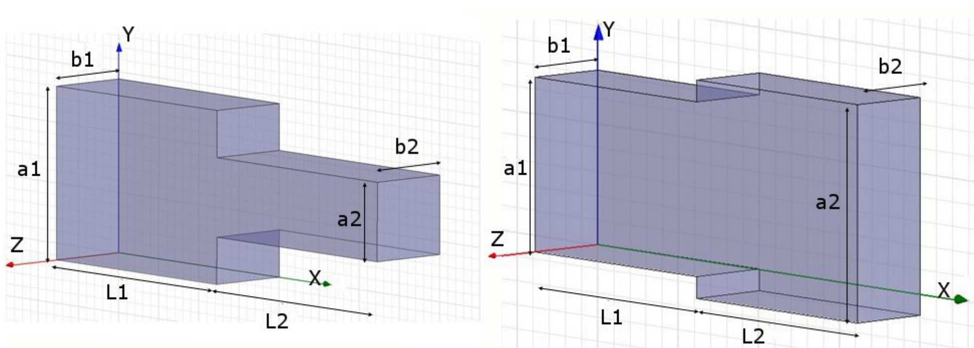

Figure 3.11: H-plane discontinuity, used for number of modes optimization. Dimensions of first waveguide are fixed: $a_1 = 0.072$m; $b_1 = 0.034$m; $L_1 = 0.1$m. Second waveguide has variable high, from $a_2 = 0.033$m (left figure) to $a_2 = 0.09$m (right figure) with 1mm step. Length and width of second waveguide are $L_2 = 0.1$m; $b_2 = 0.034$m. Applied frequency is 3.7GHz.

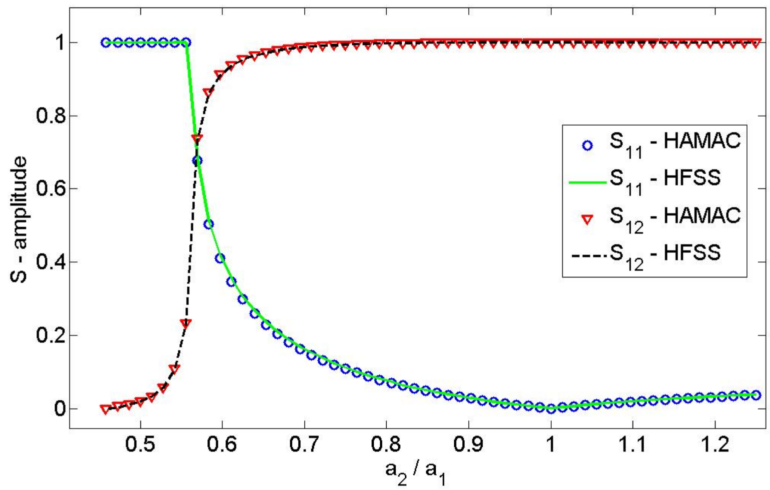

Figure 3.12: An amplitude S_{11} and S_{12} for different H-plane discontinuities. Number of TE modes is in both waveguides (see Fig. 3.11) 30. Dimensions of first waveguide are fixed: $a_1 = 0.072$m; $b_1 = 0.034$m; $L_1 = 0.1$m. Second waveguide has variable high, from $a_2 = 0.033$m to $a_2 = 0.09$m with 1mm step. Length and width of second waveguide are $L_2 = 0.1$m; $b_2 = 0.34$m. Applied frequency is 3.7GHz. We can see good agreement of HAMAC results with HFSS results.

has fixed dimensions ($a_1 = 0.072$m; $b_1 = 0.034$m; $L_1 = 0.1$m). Testing frequency is 3.7GHz. Second waveguide has changeable high: $a_2 \in \{0.033, 0.034, 0.035, \cdots, 0.09\}$m; $b_2 = 0.034$m; $L_2 = 0.1$m. S - matrix for all cases was calculated by HFSS software. Second waveguide was always centered, note that for high in the interval $0.033 - 0.071$, we model BR discontinuity, value $a_2 = 0.072$m is referring to simple straight waveguide and finally interval $0.073 - 0.09$ models BE discontinuity. Comparison of the results obtained with HAMAC code with HFSS code is presented. The aim is to find appropriate number of modes as a function of a_2/a_1. On the Fig. 3.12 we can see that with 30 modes, we have very precise result. See that for a_2 between 0.033m and 0.04m, amplitude in S_{11} is equal to 1. This means all power is reflected back, nothing is passing through discontinuity to the second waveguide output. This is because for those values of a_2, even TE_{10} mode cutoff wave number is above vacuum wave number and thus, all modes are evanescent for the frequency applied. On the contrary, for $a_2/a_1 = 1$ we get $S_{11}^{amplitude} = 0$; $S_{12}^{amplitude} = 1$, which mean no reflection at all, which is expectable since this is the case of straight waveguide.

We will compare S - matrix calculated by HFSS and HAMAC for different number of modes applied in second waveguide. We will look for a precision of 10^{-2} in amplitude and of units of degree in phase, since above this precision, we can be not sure about the accuracy of HFSS results. In first waveguide, 30 TE modes are fixed. As an example, on the Fig. 3.13 is displayed in sequence S - matrix elements for 1, 10, 20 and 30 TE modes applied in second waveguide.

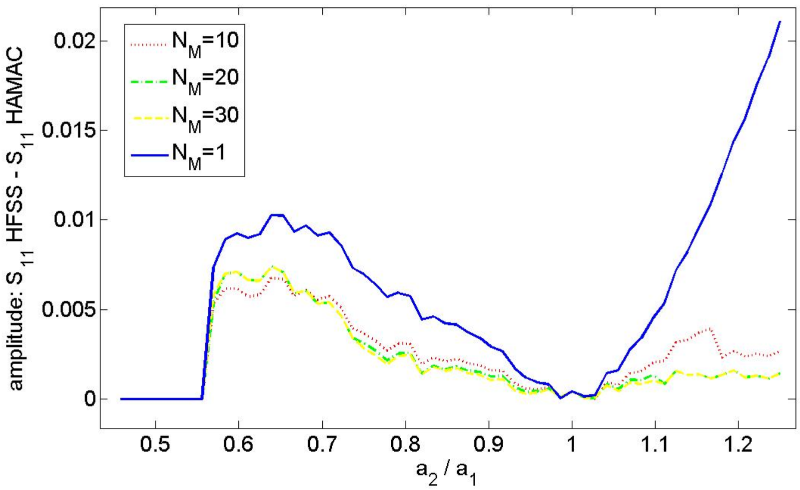

Figure 3.13: A difference of amplitude S_{11} between HFSS and HAMAC code for different H-plane discontinuities. Number of TE modes is in fixed waveguide (see Fig. 3.11) 30. We see different cases of number of TE modes forced in second waveguide. Dimensions of first waveguide are fixed: $a_1 = 0.072$m; $b_1 = 0.034$m; $L_1 = 0.1$m. Second waveguide has variable high, from $a_2 = 0.033$m to $a_2 = 0.09$m with 1mm step. Length and width of second waveguide are $L_2 = 0.1$m; $b_2 = 0.34$m. Applied frequency is 3.7GHz.

We can see that in all cases, 20 modes are sufficient and the difference between HAMAC and HFSS result is roughly smaller than 0.005. However, there is no clear behavior especially in phase, because the phase is more sensitive to the precision of HFSS calculation. Also in HAMAC calculus, there is no significant convergence when going up to 50 modes. Unfortunately, we can not conclude more than that at least 20 modes should be used. When bigger shape of waveguide appears, more modes should be needed (like in bi-junction planes).

On couple of examples, we proved the correctness of HAMAC code in comparison with HFSS. We can conclude this part to stress that presence of TM modes should be applied where the width of RF structure appears. Also, 20 modes at minimum should be taken into account. If possible, one can go with number of modes further, because (according to the theory) only the infinite number of modes should give us exact solution (note that in HFSS, we do not define any number of modes, but this software calculates in iterative loop. What we define as a criterion to stop calculus is the rate of difference of successive results). In next section, we will model in HAMAC real LH antenna to see whether the results are sustainable also in complex approach.

3.4 HAMAC validation

The HAMAC code is a plug-in module for ALOHA code. Its advantage is in straight and easy modification of parameters in order to find the desired design. In this section I first describe the design of LH antenna which is running in east China in IPP Hefei. The validation of HAMAC will be performed in the comparison with HFSS software results.

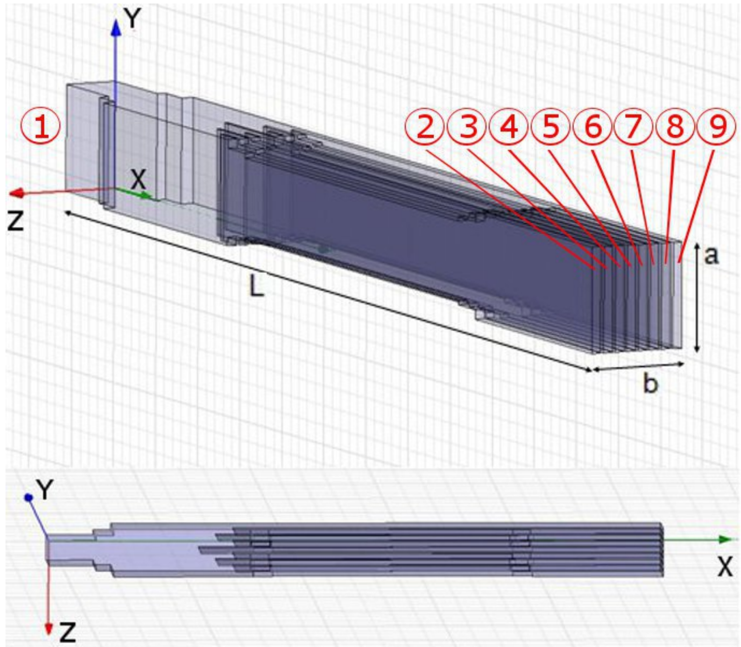

Figure 3.14: A view of one of 20 EAST 2.45GHz LH antenna module. All 9 ports are indicated. Overall parameters are $a = 0.1092$m; $b = 0.101$m; $L = 1.300$m. This module is fed by 100kW klystron.

3.4.1 LH antenna description

On EAST, there is an antenna fed by 2.45GHz. It is split into 20 equal modules. In ALOHA, there has to be adjust the antenna mouth placement. In other words, it is advantable when (and it is also for another reasons common in LHCD systems) the overall antenna is possible to be divided into several equivalent modules. In HAMAC, only one module has to be modeled since S - matrix is for each module after the same.

One of total 20 modules is shown in Fig. 3.14. Frontal view is in Fig. 3.15. Each module has 8 waveguides output, that is in total number of waveguides forming the grill mouth 160 waveguides. Each module is connected by transmission line to the 100kW klystron. Module in Fig. 3.14 is symmetric. At first, power is divided by E-plane -3dB (i.e. equally) bi-junction into two parts. Each of them is after divided further by two steps of E-plane -3dB bi-junctions, to form 8 outputs in total. The longest part of total length forms phase shifters. The phase shift on the ports 2 and 6 (see Fig. 3.14 or 3.15) is 270°, on the ports 3 and 7 is 180°, on the ports 4 and 8 is 90° and finally ports 4 and 8 are straight waveguides, i.e. phase shift is 0°. Thus, relative phase shift between two neighboring ports is 90°. The high of antenna is 0.1092m and each port in the mouth is wide 10mm. Total length of one module is 1.3m.

3.4.2 HAMAC and HFSS comparison

This design was implemented in HFSS and in order to get precise result, precise iteration was forced. Also in HAMAC, the calculation was done over first 40TE and TM modes. Both amplitude and phase reveal good agreement. In amplitude, maximal difference is 0.0099, average difference is only 0.0016. In phase, maximal difference is in S_{11} term, namely 3.4519. Still, average difference is only 0.5723.

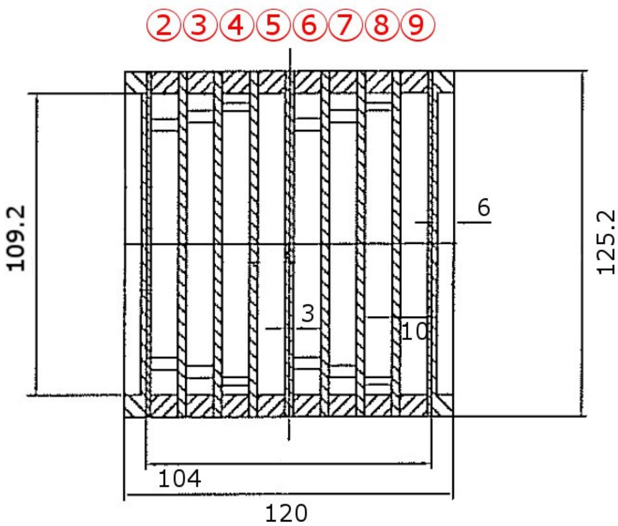

Figure 3.15: A frontal view of one of 120 EAST 2.45GHz LH antenna module. All 9 ports are indicated. Mutual phasing is set by design to 90°.

$$
\begin{aligned}
S^{amplitude}_{HFSS} &= \begin{bmatrix}
0.0591 & 0.3550 & 0.3536 & 0.3518 & 0.3515 & 0.3529 & 0.3516 & 0.3536 & 0.3534 \\
0.3550 & 0.4419 & 0.5763 & 0.3717 & 0.3727 & 0.1282 & 0.1277 & 0.1355 & 0.1354 \\
0.3536 & 0.5763 & 0.4482 & 0.3690 & 0.3700 & 0.1277 & 0.1272 & 0.1349 & 0.1348 \\
0.3518 & 0.3717 & 0.3690 & 0.4344 & 0.5936 & 0.1195 & 0.1191 & 0.1272 & 0.1271 \\
0.3515 & 0.3727 & 0.3700 & 0.5936 & 0.4331 & 0.1194 & 0.1190 & 0.1271 & 0.1270 \\
0.3529 & 0.1282 & 0.1277 & 0.1195 & 0.1194 & 0.4293 & 0.5937 & 0.3719 & 0.3729 \\
0.3516 & 0.1277 & 0.1272 & 0.1191 & 0.1190 & 0.5937 & 0.4353 & 0.3693 & 0.3703 \\
0.3536 & 0.1355 & 0.1349 & 0.1272 & 0.1271 & 0.3719 & 0.3693 & 0.4449 & 0.5774 \\
0.3534 & 0.1354 & 0.1348 & 0.1271 & 0.1270 & 0.3729 & 0.3703 & 0.5774 & 0.4435
\end{bmatrix} \\
S^{amplitude}_{HAMAC} &= \begin{bmatrix}
0.0562 & 0.3549 & 0.3535 & 0.3521 & 0.3515 & 0.3528 & 0.3514 & 0.3542 & 0.3536 \\
0.3549 & 0.4349 & 0.580 & 0.3743 & 0.3724 & 0.1275 & 0.1270 & 0.1347 & 0.1344 \\
0.3535 & 0.5810 & 0.4414 & 0.3715 & 0.3696 & 0.1270 & 0.1265 & 0.1341 & 0.1339 \\
0.3521 & 0.3743 & 0.3715 & 0.4245 & 0.5975 & 0.1197 & 0.1192 & 0.1270 & 0.1268 \\
0.3515 & 0.3724 & 0.3693 & 0.5975 & 0.4285 & 0.1195 & 0.1190 & 0.1268 & 0.1266 \\
0.3528 & 0.1275 & 0.1270 & 0.1197 & 0.1195 & 0.4229 & 0.5975 & 0.3743 & 0.3724 \\
0.3514 & 0.1270 & 0.1265 & 0.1192 & 0.1190 & 0.5975 & 0.4295 & 0.3715 & 0.3696 \\
0.3542 & 0.1347 & 0.1341 & 0.1270 & 0.1268 & 0.3743 & 0.3715 & 0.4364 & 0.5811 \\
0.3536 & 0.1344 & 0.1339 & 0.1268 & 0.1266 & 0.3724 & 0.3696 & 0.5811 & 0.4404
\end{bmatrix}
\end{aligned}
\tag{3.4}
$$

$$S^{phase}_{HFSS} = \begin{bmatrix} -8.52 & -27.32 & -117.63 & 152.98 & 63.10 & -27.22 & -117.58 & 152.70 & 62.85 \\ -27.32 & 75.29 & 141.08 & -157.96 & 112.23 & -155.54 & 114.11 & 22.93 & -66.91 \\ -117.63 & 141.08 & -105.77 & 111.67 & 21.85 & 114.14 & 23.79 & -67.39 & -157.26 \\ 152.98 & -157.96 & 111.67 & 78.03 & 141.38 & 23.33 & -67.02 & -155.30 & 114.86 \\ 63.10 & 112.23 & 21.85 & 141.38 & -101.57 & -66.56 & -156.91 & 114.82 & 24.98 \\ -27.22 & -155.54 & 114.14 & 23.33 & -66.56 & 77.22 & 140.43 & -157.87 & 112.35 \\ -117.58 & 114.11 & 23.79 & -67.02 & -156.91 & 140.43 & -103.96 & 111.72 & 21.93 \\ 152.70 & 22.93 & -67.38 & -155.30 & 114.82 & -157.87 & 111.72 & 75.94 & 142.33 \\ 62.85 & -66.91 & -157.23 & 114.86 & 24.98 & 112.35 & 21.93 & 142.33 & -103.59 \end{bmatrix}$$

$$S^{phasee}_{HAMAC} = \begin{bmatrix} -5.07 & -27.18 & -117.40 & 153.40 & 63.78 & -26.93 & -117.15 & 153.15 & 63.53 \\ -27.18 & 74.43 & 141.50 & -156.87 & 113.45 & -155.82 & 113.97 & 22.93 & -66.70 \\ -117.40 & 141.50 & -106.45 & 112.84 & 23.16 & 113.95 & 23.74 & -67.30 & -157.23 \\ 152.98 & -157.96 & 111.67 & 78.03 & 141.38 & 23.33 & -67.02 & -155.30 & 114.86 \\ 63.10 & 112.23 & 21.85 & 141.38 & -101.58 & -66.56 & -156.91 & 114.82 & 24.98 \\ -27.22 & -155.54 & 114.14 & 23.33 & -66.56 & 77.22 & 140.43 & -157.87 & 112.35 \\ -117.58 & 114.11 & 23.79 & -67.02 & -156.91 & 140.43 & -103.96 & 111.72 & 21.93 \\ 152.70 & 22.93 & -67.39 & -155.30 & 114.82 & -157.87 & 111.72 & 75.94 & 142.33 \\ 62.85 & -66.91 & -157.23 & 114.86 & 24.98 & 112.35 & 21.93 & 142.33 & -103.59 \end{bmatrix} \quad (3.5)$$

Pay attention to S_{11}term in $S^{amplitude}_{HAMAC}$ to see that only $0.0562^2 = 0.315\%$ of input power is reflected back. As far as the uniformity of output power is concerned we desire the splitting by 12.5% of power to all outputs (under estimation that no power is reflected back). Really, all terms in first row and first column (except of S_{11}) equal roughly to $\sqrt{1/8} = 0.3535$. naturally since 0.315% of power is reflected, the result is not exactly correct. See that to energy in conserved during calculus of HAMAC perfectly, because the sum of square powers of terms in first row (or in first column) gives 1.000042.

The most important parameter to compare is the phasing between neighbour waveguides. In phase of S - matrix, we can compare mutual phasing of each two neighbour output ports with theoretical prediction based on design. Phase shift between port i and j is $\Delta\phi_{ij} = S^{phase}_{i1} - S^{phase}_{j1}$. In following table, the comparison of the theoretical expectation, HFSS and HAMAC code results is done. We can see good agreement for both HFSS and HAMAC. Phase shift

$\Delta\phi_{23}$	$\Delta\phi_{34}$	$\Delta\phi_{45}$	$\Delta\phi_{56}$	$\Delta\phi_{67}$	$\Delta\phi_{78}$	$\Delta\phi_{89}$
theory						
90	90	90	90	90	90	90
HFSS						
90.31	89.40	89.87	90.33	90.36	89.71	89.85
HAMAC						
90.22	89.20	89.62	90.70	90.22	89.70	89.62

Table 3.1: Mutual phasing between 8 output ports of EAST 2.45GHz LH antenna.

calculated by HAMAC is $89.9 \pm 0.5°$, for HFSS $89.9 \pm 0.37°$. We can conclude this part by statement that HAMAC code was validated on global LH antenna design. Also we have proved that the design of $2.45GHz$ antenna is done very good since only small reflection occurs when phasing is kept almost exact $90°$, as desired.

3.4.3 ALOHA application

S - matrices presented in previous section were implemented into ALOHA. In this part, we present the resulting charts obtained by ALOHA power coupling code [6], [11]. For wave propagation frequency of 2.45GHz, the cutoff density is $0.74 \cdot 10^{17} m^{-3}$. In ALOHA, the antenna mount (grill) was depicted according to the Fig. 1.7, i.e. in four modules in toroidal direction and five modules in poloidal direction. In following charts, we present the power density spectrum for electron density $0.8 \cdot 10^{17} m^{-3}$ just in front of the grill mouth, as it was calculated by ALOHA code.

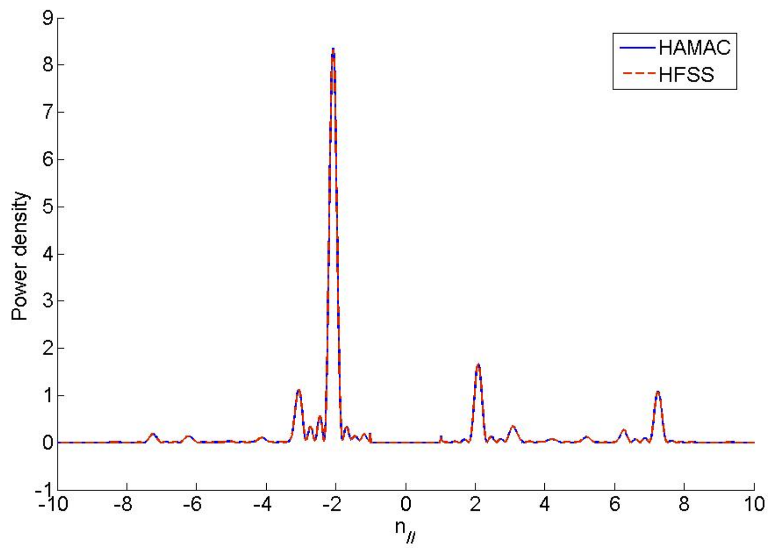

Figure 3.16: Power density spectrum of 2.45GHz LH antenna of EAST tokamak. The spectrum was calculated for electron edge density $0.8 \cdot 10^{17} m^{-3}$ by code ALOHA. S - matrix was calculated by HAMAC and HFSS software. The main peak is on $n_{\parallel} \simeq 2$.

As we mentioned in ALOHA code introduction, it is not possible to assume a vacuum layer, i.e. the plasma density in the interface of antenna grill - plasma has to be defined. From power spectrum, we can calculate the directivity, which we define here as

$$D = \frac{\int_{1}^{+\infty} dP \, \mathrm{d}n_{\parallel}}{\int_{-\infty}^{+\infty} dP \, \mathrm{d}n_{\parallel}}. \tag{3.6}$$

The power spectrum on the Fig. 3.16 is not symmetric. Also the maximum is not around $n_{\parallel} = 0$. The reason for that is the fixed mutual phasing between waveguides forming the antenna mouth. In fact, the non symmetric spectrum is the reason for waveguides phasing, since only by such spectrum, one can get the net power launched in z direction, which is the direction of plasma current in tokamak. This is the purpose of this design since it leads to current drive in tokamak vessel.

Directivity is a function of electron edge densities. In the Fig. 3.17, we see the directivity as a function of edge density. The correspondence between HAMAC and HFSS results is very good - the curves are almost identical. Directivity is for densities above cutoff ($0.74 \cdot 10^{17} m^{-3}$) approximately 75% which is very good result.

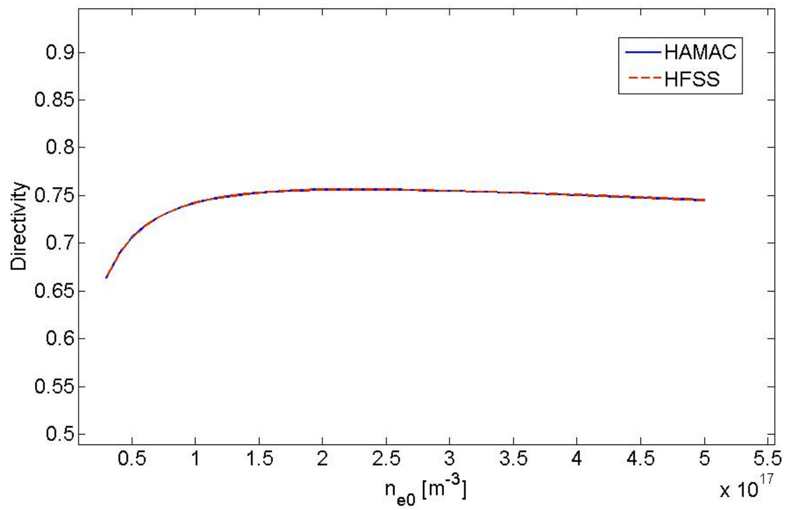

Figure 3.17: ALOHA calculation of directivity 3.6 evolution in dependence on electron edge density. S - matrix was calculated by HAMAC and HFSS software. Cutoff density for frequency used (2.45GHz) is $0.74 \cdot 10^{17} m^{-3}$.

Since directivity is calculated by integration of power spectrum (Fig. 3.16), we get almost identical result for HAMAC and HFSS, because also in power spectrum, these curves are very close each other. The reason for that is the fact that as far as power spectrum is concerned, the shape and main peak position is more sensitive to the phasing than to the whole structure of S - matrix. Thus, since the phasing is quite similar for both HAMAC and HFSS (see Tab. 3.1), we expected very close results also for spectrum.

In contrary, the reflection coefficient (Fig. 3.18) of the antenna - plasma system, being another output of ALOHA code, is very sensitive to S - matrix as a whole.

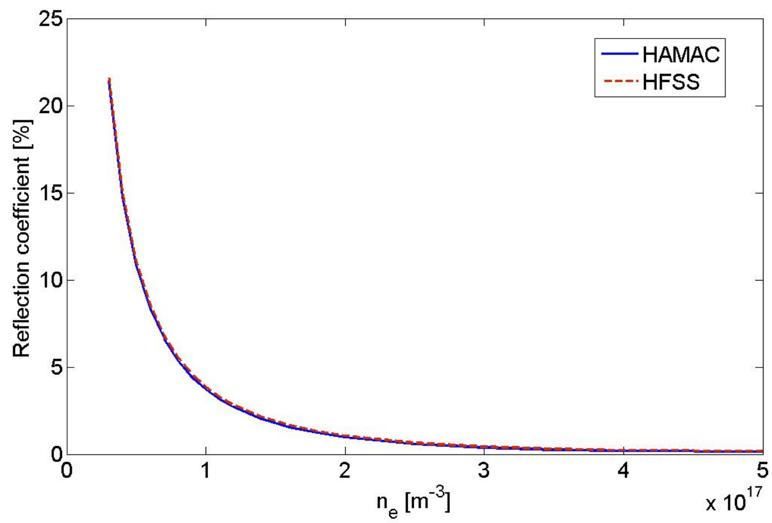

Figure 3.18: ALOHA calculation of reflection coefficient evolution in dependence on electron edge density. S - matrix was calculated by HAMAC and HFSS software. Cutoff density for frequency used (2.45GHz) is $0.74 \cdot 10^{17} m^{-3}$.

Again, the edge density is important parameter which in this case influence the reflection more than the directivity on the Fig. 3.17. For densities above cutoff density, the reflection is less than 5%. We can see again quite good correspondence of HAMAC and HFSS results. The reason is that for this antenna, I used by purpose in HAMAC code $40\,TE$ and $40\,TM$ modes. This is more than necessary, speaking about the precision - computation time ration. Repeat that in HAMAC code, usage of TM modes leads to twice longer calculation and the dependence of calculation time on number of modes used is exponential. Also in HFSS, I run calculation till the iteration difference of calculated S - matrices was under 10^{-3}. On the other hand, the convergence is in both HAMAC and HFSS very slow, but we proved on this example that HAMAC and HFSS can lead to almost identical results of both power density spectrum and reflection coefficient.

3.5 COMPASS LH antenna design

The base parameters which needs to be fulfilled in the COMPASS tokamak LH antenna is the frequency used, namely 3.7GHz. Further, the maximum possible area of the antenna grill is 140×170mm. In [13] is studied the propagation of LH waves in COMPASS tokamak environment. It is resulting in expectation of the peak of $n_\parallel$ in power spectrum between 2 and 3. We present here the results of HAMAC code S - matrices of two design trials [18, 14, 11]. Both designs suppose partition of grill mouth to 4 modules, as shown in Fig. 3.19.

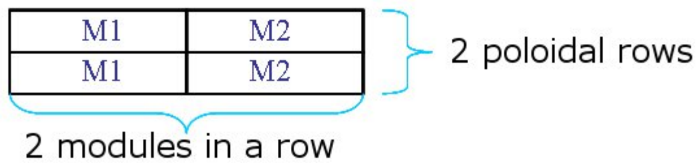

Figure 3.19: Sketch of grill antenna frontal view. Antenna mouth is divided into 4 modules.

The reason for that is the oscillation source limitation. It is expected that there will be two klystrons available. Consequently, each will feed two modules, placed on each other (poloidal direction). Thus, before the multijunction structure itself, H-plane -3dB bi-junction is needed to split the power from each klystron in poloidal direction. In this section, we will first present both trials and after see its ALOHA results, i.e. the reflection coefficient and power spectrum. In both designs, relative phase shift between two neighbour grill ports is 90°.

3.5.1 Antenna proposal No. 1

The first design counts with only 6 output waveguides per module, i.e. together 12 waveguides in two lines in poloidal direction. All the modules 1 and 2 (see Fig. 3.19) are identical. The proposed multijunction is on the Fig. 3.20. To get a phase shift between two module neighbour waveguides also 90°, there has to be the second module with the waves which are shifted by π. The thickness of all bi-junction septum (oriented in (x, y) plane) is 1mm. This is usually thickness accommodating both the minimum thickness requirements and the mechanical and thermal limitations. On the Fig. 3.20 is top view.

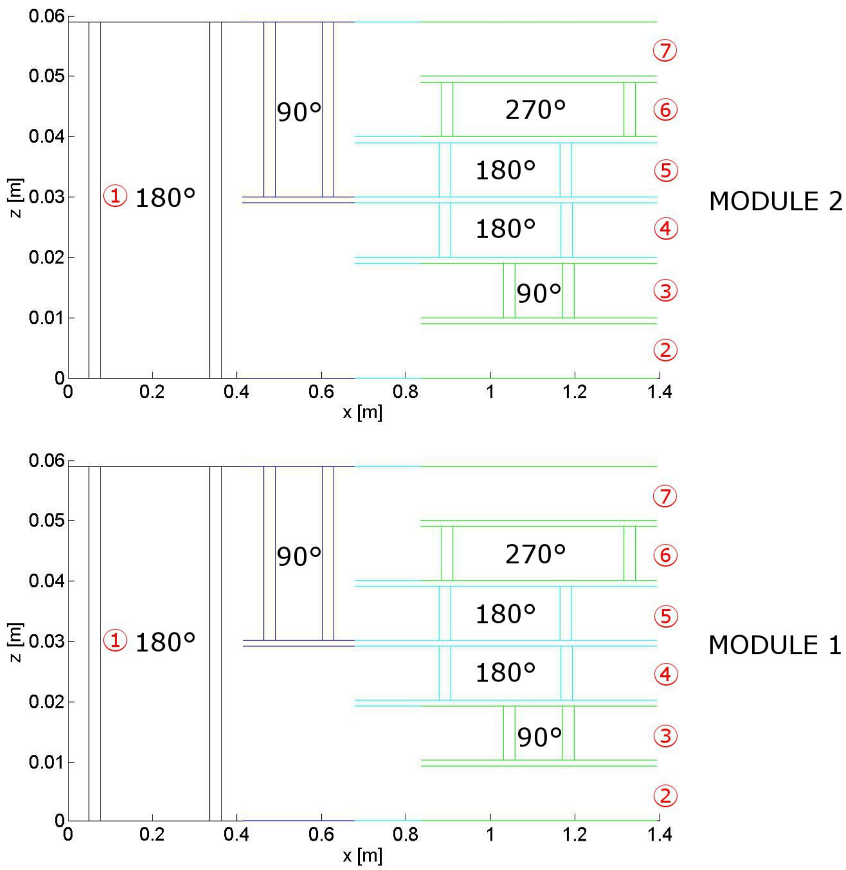

Figure 3.20: Top view of COMPASS LH antenna design supposing 2×6 output waveguides in two identical rows in poloidal direction. Thus, total number of 24 waveguides is forming the grill mouth. In red circles, number of ports is identified. Power is entering both modules in port 1.

The input waveguide cross-section is $a = 0.07$m; $b = 0.059$m and each of 6 output waveguides has a cross-section dimensions $a = 0.07$m; $b = 0.09$m. Total length is $L_{total} = 1.394$m. In Fig. 3.20, the mutual phasing is depicted to see that between output guides is the shift of 90°. In following table 3.2 is the comparison of relative phasing between output guides. Beside HFSS modeling results, one can see also results from HAMAC calculus. There are two cases for comparison purpose, one with TM and one without TM modes. See that both modules in Fig. 3.19 are separated only by 1mm thick septum, thus we can, as far as the output grill waveguide phasing is concerned, also get the mutual phasing between port number 7 of first module and port number 2 in second module. Expected result occurs. Without TM modes, the shift is not so close to theoretic value 90°. The average phase in this case is $-89.9° \pm 3.93°$. By HAMAC ($TE_{m,n}$, $TM_{m',n'}$ modes), we get resulting phasing $-90° \pm 1.5°$, to compare with HFSS result $-90° \pm 0.8°$.

3.5.2 Antenna proposal No. 2

On the contrary, this second trial fixes 8 output waveguides per module (Fig. 3.19), i.e. in total $8 \cdot 4 = 32$ waveguides forming the grill mouth in two rows per 16 guides.. Nevertheless, the grill

$\Delta\phi_{23}$	$\Delta\phi_{34}$	$\Delta\phi_{45}$	$\Delta\phi_{56}$	$\Delta\phi_{67}$	$\Delta\phi_{72}$
theory					
-90	-90	-90	-90	-90	-90
HFSS					
-90.58	-89.66	-90.66	-90.74	-88.72	-89.65
HAMAC - $TE_{m,n}$ modes					
-89.72	-88.84	-83.93	-91.61	-89.86	-96.02
HAMAC - $TE_{m,n}$, $TM_{m',n'}$ modes					
-90.05	-89.75	-87.66	-90.75	-89.42	-92.37

Table 3.2: Mutual phasing of output ports of COMPASS 3.7GHz LH antenna design with 2×6 output ports in two identical poloidal rows. In the Fig. 3.20 see numbering of ports.

area has to be the same, 140×170mm. Naturally we keep all modules the same and model in HAMAC only one of them. The thickness of all bi-junction septums (oriented in (x, y) plane) is 1mm. The same thickness we keep also between both modules in toroidal direction. Top view of one module is in Fig. 3.21.

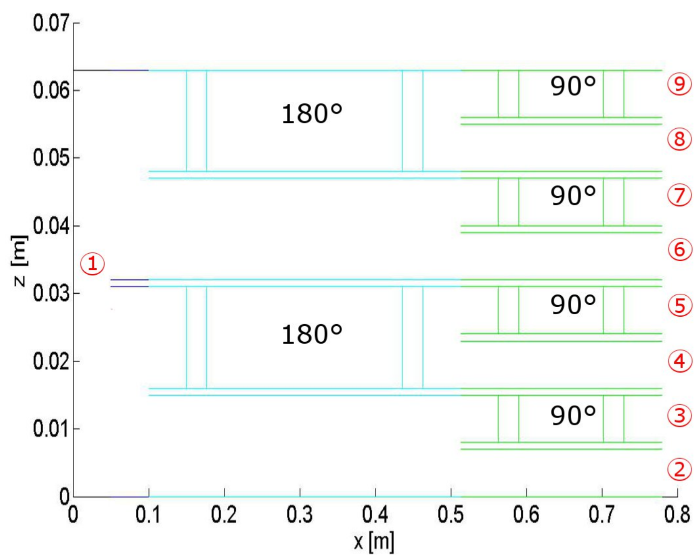

Figure 3.21: Top view of COMPASS LH antenna design supposing 2×8 output waveguides in two identical rows in poloidal direction. Thus, total number of 32 waveguides is forming the grill mouth. In red circles, number of ports is identified. Power is entering the module in port 1.

The ports are numbered too. The input waveguide cross-section is $a = 0.07$m; $b = 0.063$m, while each of 8 output waveguides has a cross-section dimensions $a = 0.07$m; $b = 0.07$m. Total length is $L_{total} = 0.7795$m. In Fig. 3.20, phase shifters used are indicated. Basic first input waveguide is after short distance split by -3dBbijunction. Subsequently the power is divided further and proper phase shifters (which dimensions are optimized by using HAMAC) are forming the output phase shift of 90°. All phase shifters are the double phase shifters, the length of all internal small waveguides are indicated by horizontal lines on Fig. 3.3. In Table 3.3, mutual phasing, calculated by HAMAC and HFSS are presented. This time I present only phasing calculated by HAMAC

$\Delta\phi_{23}$	$\Delta\phi_{34}$	$\Delta\phi_{45}$	$\Delta\phi_{56}$	$\Delta\phi_{67}$	$\Delta\phi_{78}$	$\Delta\phi_{89}$
theory						
-90	-90	-90	-90	-90	-90	-90
HFSS						
-90.01	-89.66	-90.01	-90.31	-90.01	-89.67	-90.01
HAMAC						
-90.07	-90.04	-90.07	-89.82	-90.07	-90.04	-90.07

Table 3.3: Mutual phasing of output ports of COMPASS 3.7GHz LH antenna design with 2×8 output ports in two identical poloidal rows.

with both TE and TM modes in calculus considered. The resulting phasing is $-90.03° \pm 0.09°$, to compare with HFSS result $-89, 95° \pm 0.23°$. As well as in previous design, we got with HAMAC code similar (or even better) results as with HFSS, since we can make a comparison with by theory predicted value $-90°$. On the other hand, we should run HFSS calculation in more iterations to get better results. Therefore the comparison is not so direct and we can not judge which code accords better results. In any case, for both codes, we got S - matrices which evidently correspond to expected values and both S - matrices and phase shifts can be checked by ALOHA to see the characteristics of antenna design.

3.5.3 ALOHA code results

Assuming both presented designs, we can run code ALOHA to see the resulting power spectrum, reflection coefficient and directivity of both trials. We compare three results, according to the antenna S - matrix calculus origin. All COMPASS LH antenna S - matrices were calculated by using HFSS software, HAMAC with TE and TM modes and finally HAMAC with only TE modes. In this part, we will again see the needfulness of TM modes usage. In the contrary to EAST tokamak LH antenna, in this case is the frequency used 3.7GHz and thus, cutoff density in plasma edge is $1.7 \cdot 10^{17} m^{-3}$. In following figures, we see power density spectrum for both designs.

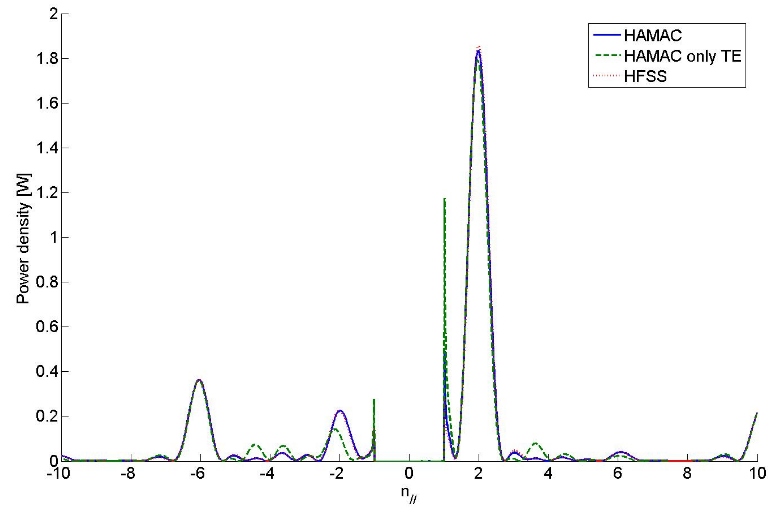

Figure 3.22: Power density spectrum of 3.7GHz COMPASS LG antenna design with 6 output waveguides per module. The spectrum was calculated for electron edge density $2 \cdot 10^{17} m^{-3}$ by code ALOHA. S - matrix was calculated by HA MAC (two cases with and without TM modes) and HFSS software. The main peak is around $n_{\parallel} \simeq 2$.

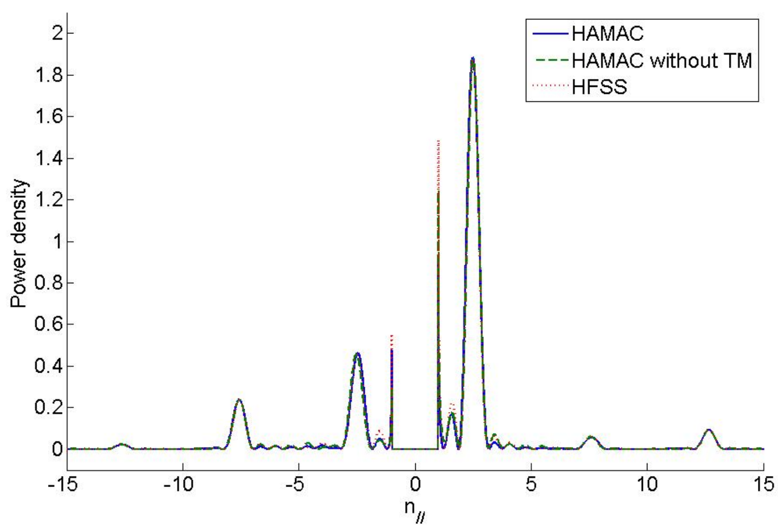

Figure 3.23: Power density spectrum of 3.7GHz COMPASS LG antenna design with 8 output waveguides per module. The spectrum was calculated for electron edge density $2 \cdot 10^{17} m^{-3}$ by code ALOHA. S - matrix was calculated by HA MAC (two cases with and without TM modes) and HFSS software. The main peak is around $n_{\parallel} \simeq 2.5$.

In case of design with 6 output waveguides, we see clear disagreement between HAMAC without TM modes results and HFSS one. Main peak is around $n_{\parallel}^{peak} \simeq 2$. On the other hand, though, in the Fig. 3.23 it is not a case. Apart from main peak, both HAMAC results reveal the shift from HFSS curve. For 8output waveguides design, peak in power spectrum is $n_{\parallel}^{peak} \simeq 2.5$. This leads to disagreement in directivity, as can be seen in Fig. 3.25, too. In case with 6 waveguides (Fig. 3.24), we can see that curves of HFSS directivity and HAMAC (with TM modes) are almost identical.

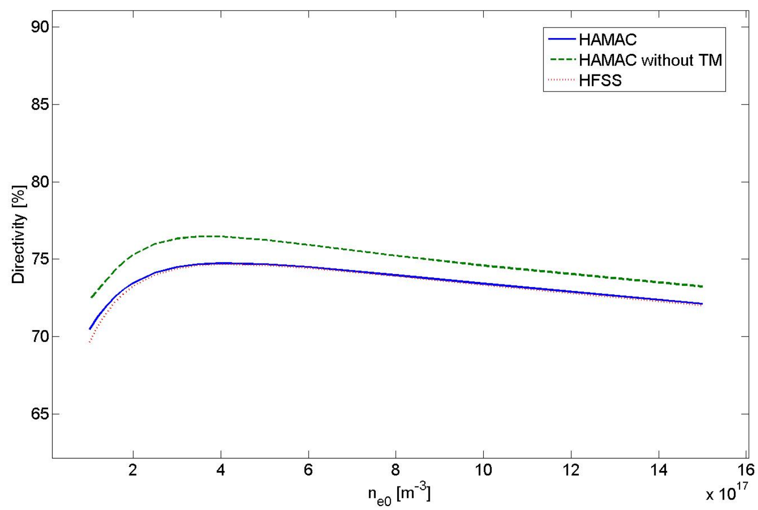

Figure 3.24: ALOHA calculation of directivity 2.41 evolution in dependence on electron edge density. Design with 6 output waveguides per module used. S - matrix was calculated by HAMAC (case with and without TM modes) and HFSS software. Cutoff density for frequency used (3.7GHz) is $1.7 \cdot 10^{17} m^{-3}$.

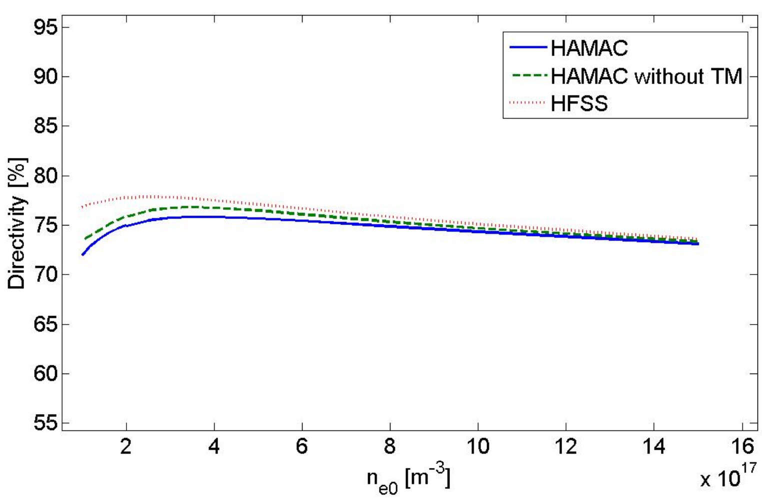

Figure 3.25: ALOHA calculation of directivity 2.41 evolution in dependence on electron edge density. Design with 8 output waveguides per module used. S - matrix was calculated by HAMAC (case with and without TM modes) and HFSS software. Cutoff density for frequency used (3.7GHz) is $1.7 \cdot 10^{17} m^{-3}$.

The problem for disagreement in design with 8 waveguides (Fig. 3.21) could be in little difference in phasing calculated (Table 3.3). In this figure, we see that HAMAC without TM modes is even closer to HFSS. Hopefully, the phasing reflect only small part of S - matrix. As we already mentioned, the S - matrix calculation precision as a whole influence more the reflection coefficient. Indeed, in Fig. 3.26 and 3.27, we see except-able results, i.e. the correspondence to HFSS curve only in case with TM modes in HAMAC.

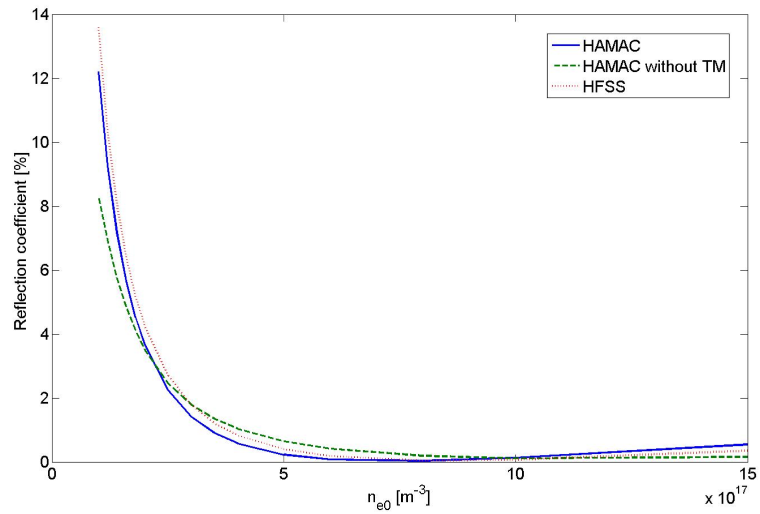

Figure 3.26: ALOHA calculation of reflection coefficient evolution in dependence on electron edge density. Design with 6 output waveguides per module used. S - matrix was calculated by HAMAC (with and without TM modes) and HFSS software. Cutoff density for frequency used (3.7GHz) is $1.7 \cdot 10^{17} m^{-3}$.

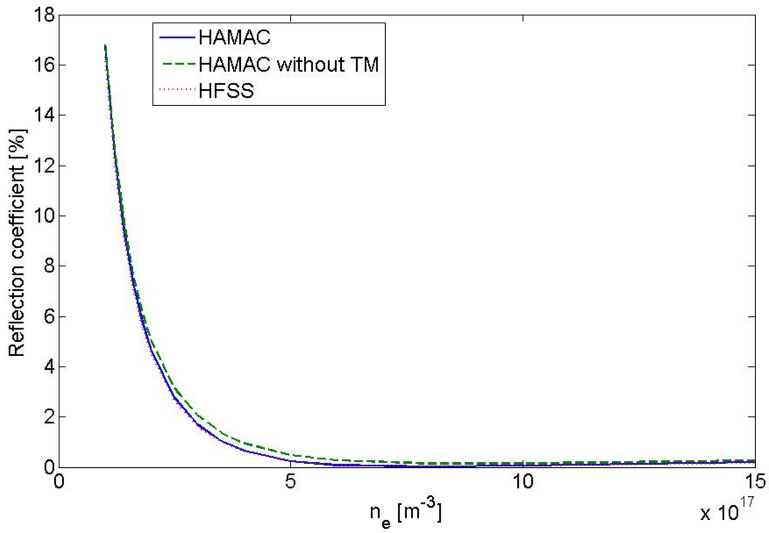

Figure 3.27: ALOHA calculation of reflection coefficient evolution in dependence on electron edge density. Design with 8 output waveguides per module used. S - matrix was calculated by HAMAC and HFSS software. Cutoff density for frequency used (3.7GHz) is $1.7 \cdot 10^{17} m^{-3}$.

Unlike the EAST design, we run this time in HAMAC only 25 modes (both in TE or TM) and in HFSS, the iteration condition was also not so severe: $\Delta S = 0.05$. Reflection coefficient in Fig. 3.26, 3.27 is calculated as an average of both modules in toroidal direction, since it is not identical for module 1 and module 2 (Coupling is different due to asymmetry of power density spectrum). We can conclude this part by statement that we saw the difference between HAMAC code calculated S - matrix when TM modes are applied or not and that both design trials are good to consider in future decision of shape of LH antenna.

Chapter 4

Summary

To fulfill the rising energy demand all around the world, the research of thermonuclear fusion power plant has to continue in both technology issues and in steady state operation issue. One of problems with the latter issue is the need of generation of plasma toroidal current. Lower Hybrid Current Drive is todays most promising tool of non-inductive current drive in tokamaks. Core of this principle is in radiation of suitable electromagnetic waves to the plasma via special launching structure called LH multijunction antenna.

Each LH multijunction antenna is basically nothing more than suitable built-up set of phase shifters and E-plane bi-junctions. Multijunction antenna is phased waveguide array, where the phase shift between two neighbour waveguides is fixed by design. The orientation in the tokamak plasma is such that the electric field vector of TE modes is parallel to the toroidal plasma current. The phasing is resulting in the presence of non zero phase velocity of radiated waves in the toroidal direction (z direction in Fig. 2.3). Thus, multijunction antenna embodies the required properties of Landau damping effect, i.e. the electric field in toroidal direction propagation and low reflection which is needed for protecting the klystrons from reflected power, especially when they are working in continuous mode such as on Tore Supra.

The design of ITER LH antenna is the issue of present research. The plan is to build the PAM antenna where the active by klystron fed waveguides alternate with so-called passive waveguides, which are short-circuited and do not radiate the power into the plasma. The advantage is the possibility of continual antenna cooling in spaces between active waveguides and also mitigation of reflected power entering back into antenna and affecting the CW klystrons. In the other hand, the active part of plasma facing antenna, i.e. the grill, is reduced by factor of 2. In this thesis we first present the introduction into the subject and also stress the needs of the LHCD upcoming research. The ALOHA code - LH wave - plasma coupling modeling code is presented. This code was developed in CEA-IRFM and is maintained presently by Dr. Julien Hillairet, CEA, Cadarache. Task of this thesis was to write a plug-in module to ALOHA: the code HAMAC presented in second chapter of this thesis was developed.

HAMAC code is written in MATLAB and its purpose is to calculate the global scattering matrix of Lower Hybrid antenna. This scattering matrix has to be known in order to run the wave - plasma coupling modeling code ALOHA. HAMAC code calculates first separately S - matrix of each simple straight waveguide as well as S - matrices of all discontinuities and junctions between those waveguides, to match them all together to create the global S - matrix, describing the antenna as a whole. In HAMAC code, the waveguides are supposed to be a perfect conductors.

Validation of HAMAC code was done on the design of EAST tokamak LH antenna system, where very good agreement between HAMAC and HFSS S - matrices was obtained. Further, the designs of future planned COMPASS tokamak LH antennas are presented.

HAMAC code contains also several optimization programs, which can be used to get the waveguide dimensions for phase shifter design e.g. Several results are presented, as well as the proof that only while TM modes are taken into account, we can get the full description of transverse E field and thus, S - matrix in better agreement to HFSS one. To prove this hypothesis was also the main object of this thesis.

Bibliography

[1] Stéphan Berio. *Développement de coupleurs ? la fréquence hybride pour la génération non inductive du courant dans un tokamak*. PhD thesis, Université d'Aix - Marseille, 1996.

[2] M. Brambilla. Slow-wave launching at the lower hybrid frequency using a phased waveguide array. *Nuclear Fusion*, 16:47–54, 1976.

[3] M. Brambilla. Waveguide launching of lower hybrid waves. *Nuclear Fusion*, 19, No.10, 1979.

[4] F. F. Chen. *Úvod do fyziky plazmatu*. Academia - ÈSAV Prague, 1984.

[5] Robert E. Collin. *Field theory of guided waves*. IEEE Press, 1991.

[6] J. Hillairet A. Ekedahl D. Voyer, M. Goniche. Advanced modeling of the coupling of lh waves to tokamak plasmas. Technical report, École Centrale de Lyon, Écully, France CEA, IRFM, Cadarache, France, 2009.

[7] T.J. Dolan. *Fusion research - Principles, Experiments and Technology*. Pergamon Press, 2000.

[8] G.T. Hoang et al. A lower hybrid current drive system for iter. *Nuclear Fusion*, 49, 2009.

[9] N. J. Fish. Confining a tokamak plasma with rf driven currents. *Physics Reviews Letters*, 41:873–876, 1978.

[10] R. Klima S. Koerbel F.Zacek, J. Preinhaelter. Sirení a útlum mimorádné vlny o frekvenci f = 2f v bezsrazkovém plazmatu zarízení tm-1-mh. Technical report, IPP, CAS, Prague, 1980.

[11] A. Ekedahl M. Goniche M. Kazda O. Meneghini D. Milanesio M. Preynas J. Hillairet, D. Voyer. Aloha: an advanced lower hybrid antenna coupling code. *Nuclear Fusion*, 50, 2010.

[12] M. Kazda. Pouziti mikrovln v termojadernem vyzkumu, 2007.

[13] M. Kazda. Neinduktivní generace elektrického proudu v tokamaku compass dolnì hybridní vlnou, 2008.

[14] M. Kazda. Improvement of hamac scattering matrix calculation code and its application to compass and east lh antennas design. Master's thesis, 2010.

[15] P. Kulhanek. Teorie plazmatu, studijní text pro fjfi, cvut, 2009.

[16] X. Litaudon. *Etude théorique et expérimentale du couplage de l'onde hybrid dans Tore-Supra et JET au moyen d'antennes a multijonctions*. PhD thesis, Université Aix-Marseille I, 1990.

[17] David M. Pozar. *Microwave engineering*. John Wiley & sons, Inc., 1998.

[18] Mélanie Preynas. Développement d'un nouveau module pour le code de couplage aloha. Master's thesis, Stage au SCCP/GCHF IRFM/CEA Cadarache, France, 2009.

[19] T. H. Stix. *Waves in plasmas*. Springer - Verlag, 1992.

[20] B. Wan and coll. Recent experiments in the east and ht-7 superconducting tokamaks. *Nuclear Fusion*, 49, 2009.

[21] John Wesson. *Tokamaks*. Clerendon Press - Oxford, 1997.

[22] M. Zaruba. Vyzaøovací struktury pro dolnì hybridní vlny - prostorové spektrum lh grilu pro tokamak compass-d. Master's thesis, FNSPE, CTU, Prague, 2007.